



A 6-DoF maneuvering model for the rapid estimation of hydrodynamic actions in deep and shallow waters

Ghalib Taimuri, Jerzy Matusiak, Tommi Mikkola, Pentti Kujala, Spyros Hirdaris*

Maritime Technology Group, Department of Mechanical Engineering, Aalto University, Espoo, Finland

ARTICLE INFO

Keywords:
Ship safety
Rapid maneuvering analysis
Reference technique
Evasiveness

ABSTRACT

We present a modular mathematical model and a reference technique for the rapid estimation of maneuvering trajectories and motion time histories of single- and twin-screw propulsion ships. Heave, roll and pitch radiation damping are estimated from a non-linear unified seakeeping/maneuvering time-domain tool using numerical decay tests and then implemented to a 6-DoF model in the form of critical damping and natural period. Short waves are idealised by numerical integration along the vessel's waterline profile and associated hydrodynamic actions are implemented in a response curve format. For the rapid assessment of hull in-plane hydrodynamic forces, derivatives are implemented via semi-empirical methods, CFD or model test data. Results are validated against experiments available for zig-zag and turning cycle trajectories of vessels with different hull forms and propulsion configurations. It is concluded that the approach presented is feasible for the prediction of maneuvering trajectories of existing or new-build vessels and for estimating the evasive velocity in way of contact before grounding.

1. Introduction

Despite progress in international maritime safety standards mitigation of risks associated with ship navigation routed accidents (e.g. collisions, groundings, etc.) remain challenging. In 2017, 3145 ship incidents and casualties were reported in EMCIP. These incidents resulted in 26 ships lost, 106 fatalities and 957 injuries (EMSA, 2019). Based on the same data records it may be concluded that from 2011 to 2016 more than 60% of casualties resulted from flooding. During this period, the passenger ship segment that represents 23% of the fleet at risk was the second highest contributor to all marine casualties. Over the same period, 172 ships sunk, primarily due to collision followed by foundering. These two categories account for almost 50% of the fatalities recorded.

These alarming accident records could be attributed to the inadequacy of safety regulations (e.g. SOLAS, 2007) to control risks associated with vessel dynamic behavior pertaining to ship design and operations under rare or extreme conditions. With the later in mind, this paper presents a rapid 6-DoF maneuvering model that could be useful for the evaluation of ship dynamic response before, during and after a hard grounding event. The method presented is original in terms of simultaneously evaluating (1) coupled heave/pitch and roll ship

motions, (2) velocities in way of contact, (3) 6-DOF evasive maneuvers in a way that accounts for all pertinent phenomena involved along a ship's traveled path (e.g. waves, shallow water effects) and applies to modern single- and twin-screw vessels. Selected key ship parameters of relevance to ship evasiveness and associated navigation routed accidents in restricted waters are taken under consideration. Such conditions may be representative of many collision and grounding events (Kujala et al., 2009; Pagiaziti et al., 2015; Schröder-Hinrichs et al., 2012).

For completeness, the effects of shallow water, short waves, different propulsion and steering arrangements on maneuvering motions are discussed in detail. The new elements of the method are verified, and the method is validated using three well-documented experiments that represent different rudder/propeller combinations (Chilcree and el Moctar, 2018; SIMMAN, 2020) and data of modern Twin Propeller Twin Rudder (TPTR) passenger vessel provided by a shipyard.

2. Literature review

Since the 1970's various mathematical models have been derived and validated with the aim to represent the influence of maneuvering and seakeeping motions on ship dynamics (Beck et al., 1989; ITTC, 2017a; Matusiak, 2017). Traditionally maneuvering dynamics have

* Corresponding author.

E-mail address: syros.hirdaris@aalto.fi (S. Hirdaris).

Nomenclature	
CFD	Computational Fluid Dynamics
CoG	Center of Gravity
DOF	Degrees of Freedom
DTC	Duisburg Test Case
DTMB	David Taylor Model Basin
EEDI	Energy Efficiency Design Index
EMCIP	European Marine Casualty Information Platform
EMSA	European Maritime Safety Agency
FEA	Finite Element Analysis
FSB	Floodstand Ship B
FSI	Fluid-Structure Interaction
IMO	International Maritime Organization
ITTC	International Towing Tank Conference
KRISO	Korea Research Institute of Ships and Ocean Engineering
KVLCC2	KRISO Very Large Crude Carrier - 2
MMG	Maneuvering Modeling Group
ONRT	Office of the Naval Research Tumblehome
PMM	Planar Motion Mechanism
RANS	Reynolds Average Navier-Stokes
SOLAS	Safety of Life at Sea
SPSR	Single propeller and single rudder
TPTR	Twin propeller and twin rudder
A_e/A_0	Blade area ratio
A_L, A_T	Lateral and transversal area of ship structure above waterline (m^2)
A_{Rmov}	Lateral moveable rudder area (m^2)
A_{wp}	Waterplane area (m^2)
a_H	Coefficient of increase lateral force at rudder due to the presence of hull
B	Beam of the ship (m)
C_B	Ship block coefficient
C_{D0}	Rudder frictional drag coefficient
C_L, C_D	Rudder lift and drag coefficient
C_T	Ship resistance coefficient
C_{Th}	Thrust loading coefficient
C_{rud}	Rudder cord length (m)
$C_v, C_{v_{deep}}$	Viscous coefficient in shallow and deep water
D	Diameter of the propeller (m)
D_S	Steady turning circle diameter (m)
F_n	Froude number
F_{qs}	Centrifugal force in a steady turning circle (N)
GM_{T0}, GM_{L0}	Transverse and longitudinal initial metacentric height
g	Acceleration of gravity (9.807 m/s^2)
H	Depth of the sea (m)
I_X, I_Y, I_Z	Roll, pitch and yaw moment of inertia (kg m^2)
KG	Vessels' Center of gravity measured from keel (m)
K, M, N	hydrodynamic moments acting on ship hull in the body fixed co-ordinate system (Nm)
K_{Hull}	External roll added damping Moment (Nm)
K_{rud}	Rolling moments on rudder in body-fixed system (Nm)
K_{SW}	Short waves roll moment (Nm)
K_p	Variation of roll moment due to roll acceleration (Nms^2)
K_r	Variation of roll moment due to yaw acceleration (Nms^2)
K_v	Variation of roll moment due to sway acceleration (Nms^2)
k	Wave number ($2\pi/\lambda$)
k_{T0}, k_{T1}, k_{T2}	2nd order polynomial propeller thrust characteristics coefficients
L_{pp}	Length between perpendiculars (m)
M_{rud}	Pitching moments on rudder in body-fixed system (Nm)
M_q	Variation in pitch moment due to pitch acceleration (Nms^2)
m	Mass of the ship (kg, tons)
N_{Hull}	External yaw added damping moment (Nm)
N_p	Number of propellers
N_{rud}	Yawing moments on rudder in body-fixed system (Nm)
N_{SW}	Short waves yaw moment (Nm)
$N_{\dot{y}}$	Variation in yaw moment due to sway acceleration (Ns^2)
$N_{\dot{r}}$	Variation in yaw moment due to yaw acceleration (Nms^2)
n	Propeller revolution (rps)
N'_v, N'_r	Effect of sway and yaw linear velocities on yawing moment
N'_{vv}, N'_{rr}	Changes in yaw moment due to higher-order pure sway velocity and yaw velocity
N'_{vrr}, N'_{vvr}	Coupled effect of sway and yaw velocity on yaw moment
p, q, r	Angular (roll, pitch & yaw) velocities in the body fixed coordinate system (m/s)
$\dot{p}, \dot{q}, \dot{r}$	Angular (roll, pitch & yaw) acceleration in the body-fixed coordinate system (rad/s^2)
R_n, R_{n+1}	Consecutive peaks of undamped response
r_0	Radius of the propeller (m)
r_{inf}	Slipstream radius far downstream (m)
r_x	Slipstream radius at rudder centroid (m)
S_R	Rudder total wetted area (m^2)
S_W	Wette surface area of ship (m^2)
T	Ship draft (m)
t	Thrust deduction factor
U, u	Instantaneous ship speed (m/s)
u, v, w	Translational (surge, sway & heave) velocities in body-fixed coordinate system (m/s)
$\dot{u}, \dot{v}, \dot{w}$	Translational (surge, sway & heave) acceleration in body-fixed coordinate system (rad/s^2)
V_A	Propeller advance velocity (m/s)
V_{corr}	Velocity correction in propeller slip stream due to turbulent mixing of the flow (m/s)
V_{inf}	Propeller wash axial velocity far downstream (m/s)
V_S	Steady turning circle velocity (m/s)
V_x	Velocity of propeller flow in slipstream region (m/s)
$V_{X,R}$	Axial flow velocity at rudder (m/s)
$V_{Y,R}$	Radial flow velocity at rudder (m/s)
w	Wake fraction at propeller
X_{Hull}	External surge fluid damping forces (N)
X_{prop}	Propeller Thrust (N)
X_{res}	Clam water resistance (N)
X_{rud}	Rudder drag forces (N)
X_{SW}	Short waves surge forces (N)
$X_{\dot{u}}$	Variation in longitudinal force due to surge acceleration (Ns^2/m)
$X'_{vr}, X'_{vv}, X'_{rr}, X'_{vrv}, X'_{vvv}$	X-directional resistance addition due to ship motions in pure sway, pure yaw and coupled influence of sway and yaw velocities in the longitudinal direction
x_F	Center of floatation (m)
x_G	Longitudinal distance of the center of gravity measured from midship (m), +ve bow (m)
x_P, x_R	Longitudinal position of propeller and rudder from midship respectively
X, Y, Z	hydrodynamic forces acting on ship hull in the body fixed co-ordinate system (N)
$\dot{X}_G, \dot{Y}_G, \dot{Z}_G$	Translational velocities in Earth fixed system (m/s)
Y_{Hull}	External sway fluid damping forces (N)
Y_{rud}	Rudder lift forces (N)
Y_{SW}	Short waves sway forces (N)
$Y_{\dot{p}}$	Variation in lateral force due to roll acceleration (Ns^2)
Y_r	Variation in lateral force due to yaw acceleration (Ns^2)
$Y_{\dot{v}}$	Variation in lateral force due to sway acceleration (Ns^2/m)
Y'_v, Y'_r	Effect of sway and yaw linear velocities on lateral force
Y'_{vrr}, Y'_{vvr}	Coupled effect of sway and yaw velocity on sway force and

Y'_{vvv}, Y'_{rrr}	yaw moment Changes in lateral force (Y') and yaw moment (N') due to higher-order pure sway velocity and yaw velocity
Z_q	Variation in heave force due to pitch acceleration (Ns^2)
Z_w	Variation in heave force due to heave acceleration (Ns^2/m)
z_G	Vertical distance of the center of gravity measured from midship and still waterline +ve towards keel (m)
z_R	Location of rudder centroid measured from waterline (m)
O – X, Y, Z	Earth fixed coordinate system
$o - x, y, z$	body-fixed coordinate system
α	Effective angle of attack of the flow at rudder (rad, deg) Angle between normal of the waterline and wave crest
α_T	Draft correction factor in shortwaves
β	Drift angle amidships (rad, deg)
β_R	Flow drift angle at rudder (rad, deg)
β_w	Wave direction in the earth-fixed coordinate system (rad, deg), 180° is head waves
γ_R	Flow-straightening coefficient
Δr	Increase in slipstream radius due to turbulence of the flow (m)
Δz	Instantaneous change in heave displacement (m)
δ	Rudder angle (rad, deg), +ve portside
δ_{lim}	Limiting rudder angle (deg, rad)
δ_T	Target rudder angle (deg, rad)
$\dot{\delta}$	Change in rudder angle with respect to time (rad/sec)
ζ_a	Wave amplitude (m)
$\zeta_w, \zeta_\phi, \zeta_\theta$	Heave, roll and pitch damping ratios
θ	Angle between tangent to the waterline and longitudinal axis (rad, deg)
Λ_{eff}	Effective aspect ratio
Λ_{geom}	Geometric aspect ratio
λ	Diminishing rudder lift factor
ρ	Water density (kg/m^3)
$\dot{\varphi}, \dot{\theta}, \dot{\psi}$	Angular velocities in Earth fixed system (rad/s)
ψ	Heading angle, yaw (rad, deg)
ω_0	Circular wave frequency (rad/sec)
ω_δ	Rudder rate (rad/sec)
$\omega_w, \omega_\phi, \omega_\theta$	Heave, roll and pitch angular frequencies

been modeled in calm seas (i.e. sheltered waters or harbor conditions) and aimed to define ship behavior following an operator's decision. On the other hand, the development of seakeeping methods focused on the evaluation of motions in waves in the absence of any control in-plane actions. Multi-DoF unified seakeeping/maneuvering theories have been developed progressively and applied to cases of specialist intact ship stability phenomena (Spyrou et al., 2000), ship overtaking scenarios (Yu et al., 2019) or solvers used to simulate ship dynamic behavior in real conditions (Matusiak, 2017). Modern methods use the so-called Maneuvering Modeling Group (MMG) standard methodology (Yasukawa and Yoshimura, 2015). They also make use of time-domain approaches that combine various levels of hydrodynamic nonlinearity (Hirdaris et al., 2016).

Key academic developments of relevance to this paper can be summarized in two groups namely: (i) the derivation and validation of unified models that simulate ship operations in deep or shallow waters under varying environmental assumptions and (ii) improved idealization of the effects of evasive ship dynamics pertaining to accidental events (collisions, groundings, etc.).

With reference to the former various 4- and 6-DoF models have been derived. For example, (Perez et al., 2007), proposed a 4-DoF maneuvering model using the equations of motion presented in (Fossen, 2002). In their work, a genetic algorithm has been used to adjust the maneuvering parameters initially estimated from the 2.5D seakeeping approach of (Faltinsen and Zhao, 1991). (Seo and Kim, 2011), presented the numerical analysis of ship maneuverability in regular waves. In this work Froude-Krylov, diffraction, radiation and 2nd order mean drift forces were estimated by a Rankine panel method and hydrodynamic actions were added into the maneuvering model as external forces. A similar model has been introduced by (Sprenger et al., 2017), who assessed the optimum maneuverability of ships to ultimately satisfy EEDI requirements (IMO, 2013). In their work, they also accounted for 2nd order hydrodynamic actions that may influence the water resistance and maneuvering derivatives in calm waters. This approach has been extended by (Tillig and Ringsberg, 2018) to account for the effects of vessel drift and rudder angle when resistance in waves is accounted for. With reference to 6-DoF models, notable developments have been limited. The unified model presented by (Bailey et al., 2002) remains topical. The method combines frequency domain Green function seakeeping dynamics in random or irregular seaways with a linear convolution integral to account for the influence of unsteady memory effects during ship maneuvering in waves. Although the model is mathematically robust, wave prediction is not exact. Also, computations may be

lengthy for use in practical applications primarily because of time variations related to the encounter frequency and heading angles. These practical implementation issues are also of relevance to the more recently presented model of (Chilcée and el Moctar, 2018). Their approach makes use of a Rankine panel method and hydrodynamic coefficients by RANS PMM tests in calm waters and regular waves. The method of Matusiak (2017) combines maneuvering with a time-domain non-linear seakeeping model in a single set of coupled equations of motion that are solved simultaneously. Convolution terms are used to represent the memory effect of radiation forces in heave, pitch and roll. Empirically derived coefficients of in-plane motion components are utilized. This model has been applied to reveal the occurrence of large amplitude roll motions in stern quartering irregular seas during a turning maneuver (Acanfora and Matusiak, 2014; Matusiak and Stigler, 2012). In the model by Matusiak (2017) external hydrodynamic forces acting on the hull are represented by empirical hydrodynamic coefficients. A beneficial method that may be used to assess the credibility of those on maneuvering is sensitivity analysis over a range of vessels progressing along various maneuvering trajectories (e.g. see Gavrilin and Steen, 2018 and Sukas et al., 2019). Such approach is considered beneficial in terms of qualifying uncertainties associated with modelling and simulation assumptions.

With reference to shallow water effects key developments on the influence of ship maneuvering forces and moments have been introduced by (Vantorre, 2001), (Vantorre et al., 2017), (Rotteveel, 2013) and (Liu et al., 2015). These authors highlighted the importance of ship resistance in shallow and confined waters. Accordingly, it is understood that in restricted conditions (i) the tactical diameter of vessels may enlarge especially due to hull damping effects; (ii) increases in ship resistance may lead to decrease in maneuvering capability and (iii) changes in pressure hull distributions may lead to increased hydrodynamic forces.

Whereas advances in marine hydrodynamics look promising, work on evasive ship dynamics pertaining to accidental events (collisions, groundings, etc.) is still very limited and subject to both computational uncertainties and costs (Varsta et al., 2004a, 2004b). coupled a 6-DoF ship dynamics model with a simplified contact model representing hard grounding (Ståhlberg et al., 2013). highlighted the importance of ship velocity and time history in determining vessel evasive maneuvers in case of collision (Yu and Amdahl, 2016). presented a coupled approach for simultaneously calculating structural damage and the 6-DoF ship motions in ship collisions.

None of these studies focused on the development of rapid assessment tools that account for the combined influence of seakeeping and

maneuvering induced dynamics on vessel response during both grounding and collision events. Recently (Kim et al., 2020) introduced a 3D FSI model coupling explicit FEA structural dynamics with seakeeping, maneuvering and calm water resistance. This work re-affirmed the importance of developing simplified and accurate tools with the aim to practically implement the influence of multiphysics modelling assumptions on ship structural crashworthiness and associated rule development.

3. Theory

The rigid body time domain 6-DoF rapid assessment model introduced in this paper is based on the following assumptions:

- (i) Hull in-plane forces are represented by quasi-steady flow reactions and described by non-dimensional coefficients referring to motion velocities and accelerations.
- (ii) Short waves are modeled according to (Faltinsen, 1990) and (Sakamoto and Baba, 1986).
- (iii) Shallow water idealisations account for increase in ship resistance, changes in added mass/damping as well as changes in flow-straightening coefficient, wake fraction and thrust deduction factors.
- (iv) Heave, pitch and roll motions are assumed to be small and represented by the linear relations of forces and motion components. These are not affected by shallow water. Thus, out of plane motions are small and GM_{T0}/GM_{L0} are assumed constant.
- (v) The action of short waves is restricted to in-plane motions. Thus, the wave-induced heave, pitch and roll are assumed to be negligible.
- (vi) For computational economy memory effects are not taken under consideration.

3.1. Motions

The translational velocities of surge (u), sway (v) and heave (w) and rotational degrees of freedom namely roll (p), pitch (q) and yaw (r) are shown in Fig. 1. The earth fixed coordinate system is represented as $O - XYZ$. The body-fixed coordinate system $o - xyz$ is attached amidships ($L_{pp}/2$) at a distance x_G positive toward the bow. Accordingly, it rests on the still waterline passing through the vessel symmetry plane ($x-z$), with the longitudinal (x) axis pointing positive towards the bow, the lateral (y) axis directed towards the starboard side and the vertical (z) axis pointing downwards. The ship heading forms a positive angle ψ from the earth-fixed X -axis to the body-fixed x -axis. The drift angle β is defined at amidships with

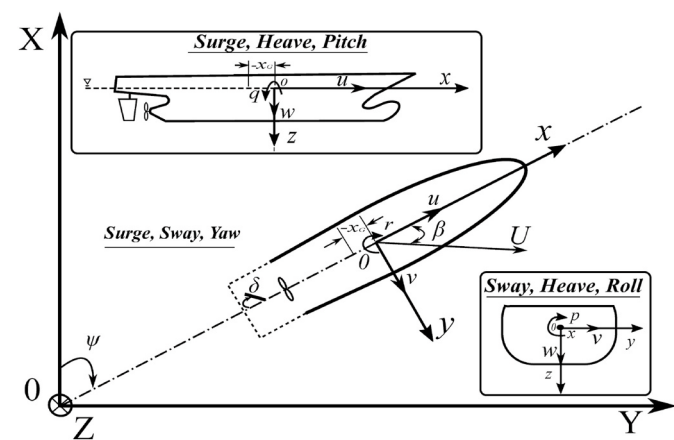


Fig. 1. Coordinate system representing 6-DOF motions of a ship.

translational and angular velocities are transformed from the body-coordinate to inertial-coordinate systems as per Fossen (2011). Accordingly, the coordinate transformation (see Eq. (1)), is embedded as a sub-block of the 6-DoF maneuvering model (see Fig. 6). The general form of rigid body motion comprises of translation and rotation DoF governed by Newton's 2nd law of motion. Thus, forces representing the external loading action on the ship when she progresses with some forward speed are expressed by the conservation of linear and angular momentum. In principle, hydrodynamic forces act on the CoG of the ship with respect to an inertial frame of reference. It is difficult to express external forces in such a manner. Hence, the body-fixed coordinate system was defined, which is transformed into the inertial frame of reference as:

$$\begin{aligned} \dot{x}_G &= u\cos(\psi)\cos(\theta) + v[\cos(\psi)\sin(\theta)\sin(\phi) - \sin(\psi)\cos(\phi)] \\ &+ w[\sin(\psi)\sin(\phi) + \cos(\psi)\cos(\phi)\sin(\theta)] \dot{Y}_G = usin(\psi)\cos(\theta) \\ &+ v[\cos(\psi)\cos(\phi) + \sin(\phi)\sin(\theta)\sin(\psi)] \\ &+ w[\sin(\theta)\sin(\psi)\cos(\phi) - \cos(\psi)\sin(\phi)] \dot{Z}_G = -usin(\theta) + v\cos(\theta)\sin(\phi) \\ &+ w\cos(\theta)\cos(\phi)\dot{\phi} = p + q\sin(\phi)\tan(\theta) + r\cos(\phi)\tan(\theta)\dot{\theta} = q\cos(\phi) \\ &- rsin(\phi)\dot{\psi} = q\frac{\sin(\phi)}{\cos(\theta)} + r\frac{\cos(\phi)}{\cos(\theta)} \end{aligned} \quad (1)$$

Maneuvering models normally consider that the origin of the body-fixed system is not on the CoG but amidships. Therefore, the equation of translational and rotational motions was modified as:

$$\begin{aligned} (m - X_u)\dot{u} + (mz_G - 0.5 X_u T)\dot{q} &= mrv + mx_G(r^2 + q^2) - mwq - mz_Gpr + \rho g A_{WP}(\Delta z)\sin(\theta) + X_{Hull} + X_{Res} + X_{Prop} + X_{Rud} + X_{Wind} + X_{SW} \\ (m - Y_v)\dot{v} - (mz_G + Y_p)\dot{p} + (mx_G - Y_r)\dot{r} &= m(pr - ru - z_Gqr - x_Gpq) - \rho g A_{WP}(\Delta z)\sin(\phi)\cos(\theta) + Y_{Hull} + Y_{Rud} + Y_{Wind} + Y_{SW} \\ [(m - Z_w)\dot{w} - (mx_G + Z_q)\dot{q}] &= m(uq - vp + z_G(p^2 + q^2) - x_Grp) - \rho g A_{WP}(\Delta z)\cos(\phi)\cos(\theta) + \rho g A_{WP}x_F\theta] - 2\zeta_w\omega_w w \\ [-(mz_G + K_v)\dot{v} + (I_x - K_p)\dot{p} + (mx_Gz_G - K_r)\dot{r}] &= m(z_Gur - z_Gwp - x_Gzp) + (I_y - I_z)qr - mgGM_{T0}\sin(\phi)\cos(\phi)\cos(\theta) + K_{Hull} + K_{Rud} + K_{SW}] - 2\zeta_\phi\omega_\phi p \\ [(mz_G - 0.5 X_u T)\dot{u} - (mx_G + Z_q)\dot{w} + (I_y - M_q)\dot{q}] &= m(z_Gvr - z_Gwq + x_Gvp - x_Guq + x_Gz_g(p^2 - r^2)) + (I_z - I_x)pr - mgGM_{L0}\sin(\theta)\cos(\phi)\cos(\theta) \\ + \rho g A_{WP}x_F\Delta z + M_{Rud}] &- 2\zeta_\theta\omega_\theta q(mx_G - N_v)\dot{v} - (mx_Gz_G - K_r)\dot{p} + (I_z - N_r)\dot{r} = m(x_Gwp - x_Gur + x_Gzp) + (I_x - I_y)pq - \rho g\nabla(-GM_{L0}\cos(\theta) \\ + GM_{T0})\sin(\phi)\sin(\theta) + N_{Hull} + N_{Rud} + N_{Wind} + N_{SW} \end{aligned} \quad (2)$$

respect to the ship's longitudinal and lateral velocity vectors. The rudder angle δ is positive towards the port side. The change of the course of the ship (ψ) is positive during the starboard turn, where the rudder angle is negative.

The ship position is established in the earth-fixed coordinate system using a transformation-rotation matrix corresponding to the rotation angles φ, θ and ψ about x , y and z -axis respectively (see Fig. 1). The

In Eq. (2) the left-hand side terms correspond to the inertia of the ship including added masses and moments of inertia. The mass multiplier terms on the right-hand side are the Coriolis and centripetal forces. The terms multiple of "g" represent the hydrostatic forces as per (Fossen, 2011) and (Lewandowski, 2004). The remaining terms describe damping, control and

environmental forces discussed in subsequent sections 3.2–3.7. The hydrostatic terms in surge, sway and yaw do not affect in-plane motions. Instead, they are activated by heave, roll and pitch motion components caused by grounding. Mass multipliers on the right hand side of Eq. (2) reflect the influence of Coriolis and centripetal forces on maneuvering. The linear model of heave, pitch and roll motion components given by Eq. (2) requires the knowledge of natural periods and critical damping ratios. The natural frequencies of heave, pitch and roll motions are presented as follows:

$$\begin{aligned}\omega_w &= \sqrt{\frac{\rho g A_{wp}}{m - Z_{\dot{w}}}} \\ \omega_\varphi &= \sqrt{\frac{mg GM_T}{I_x - K_p}} \\ \omega_\theta &= \sqrt{\frac{mg GM_L}{I_y - M_{\dot{q}}}}\end{aligned}\quad (3)$$

The damping ratios ζ_w , ζ_φ and ζ_θ were evaluated by applying the nonlinear time domain 6-DoF solver LaiDyn of Matusiak (2017). They were evaluated by releasing the ship from an initial input excitation encompassing heave-displacement as well as roll and pitch angles and performing numerically a decay test. The critical damping ratio was evaluated as:

$$\zeta_{w,\varphi,\theta} = \frac{1}{2\pi} \ln \left(\frac{R_n}{R_{n+1}} \right), \quad (4)$$

3.2. Hull resistance and propulsion

The model assumed calm water resistance in a straight course with no drift as follows:

$$X_{res} = -0.5\rho U^2 S_w C_T / (1-t) \quad (5)$$

The initial thrust of the propeller was modeled as the power required to overcome hull resistance according to the equation:

$$X_{Prop} = -\frac{X_{res}}{N_P} \quad (6)$$

Constant propeller revolutions were then predicted as:

$$n = \frac{-k_{T1} V_A \rho D^3 + \sqrt{(k_{T1} V_A \rho D^3)^2 + 4k_{T0} \rho D^4 (V_A^2 \rho D^2 k_{T2} - X_{Prop})}}{2k_{T0} \rho D^4} \quad (7)$$

Assuming the propeller wake is constant throughout the maneuvering motion the instantaneous propeller thrust was defined as:

$$X_{Prop} = \rho n^2 D^4 (K_T) \quad (8)$$

$$\text{for } K_T = k_{T0} + \frac{k_{T1} V_A}{D} + k_{T2} \left(\frac{V_A}{D} \right)^2 \quad (9)$$

$$\text{and } V_A = (1-w) U \quad (10)$$

3.3. Rudder forces

3.3.1. Single propeller single rudder (SPSR) configuration

To estimate the slipstream radius, the distance between the propeller plane and the rudder center of gravity was defined according to (Brix, 1993). The axial velocity far downstream of the propeller plane and the thrust loading coefficient were defined as:

$$\begin{aligned}C_{Th} &= \sqrt{\frac{8n^2 D^2 K_T}{\pi V_A^2}} \\ V_{inf} &= V_A \sqrt{1 + C_{Th}}\end{aligned}\quad (11)$$

The propeller slipstream velocity at the rudder was predicted from

momentum theory and the slipstream radius behind the propeller and axial velocity were evaluated as:

$$\begin{aligned}r_{inf} &= r_0 \sqrt{\frac{1}{2} \left(1 + \frac{V_A}{V_{inf}} \right)}, \text{ where } \left\{ r_0 = \frac{D}{2} \right\} \\ r_x &= r_0 \frac{0.14 \left(\frac{r_{inf}}{r_0} \right)^3 + \frac{r_{inf}}{r_0} \left(\frac{|x_R - x_P|}{r_0} \right)^{1.5}}{0.14 \left(\frac{r_{inf}}{r_0} \right)^3 + \left(\frac{|x_R - x_P|}{r_0} \right)^{1.5}} \\ V_x &= V_{inf} \left(\frac{r_{inf}}{r_x} \right)^2\end{aligned}\quad (12)$$

Turbulent mixing attributed to the complex geometry of the propeller blades, body and hub diameter in way of the fluid flow were defined as:

$$\begin{aligned}\Delta r &= 0.15 |x_R - x_P| \frac{V_{inf} r_{inf}^2 - V_A r^2}{V_{inf} r_{inf}^2 + V_A r^2} \\ V_{corr} &= (V_x - V_A) \frac{r^2}{(r_x + \Delta r)^2} + V_A\end{aligned}\quad (13)$$

Longitudinal and lateral flow velocities on the rudder were defined according to (Matusiak, 2017) as:

$$\begin{aligned}V_{X,R} &= V_{corr} + q z_R + y_R r \\ V_{Y,R} &= -v - r x_R + p z_R\end{aligned}\quad (14)$$

In turn, rudder forces were estimated according to (Matusiak, 2017) and the interaction between the root of the rudder and the body of the ship was defined according to (Molland and Turnock, 2007) as follows:

$$\begin{aligned}X_{Rud} &= -0.5 C_D \rho (V_{X,R}^2 + V_{Y,R}^2) A_{RUD} \cos(\gamma_R \beta_R) \\ &\quad + 0.5 C_L \rho (V_{X,R}^2 + V_{Y,R}^2) A_{RUD} \sin(\gamma_R \beta_R) \\ Y_{Rud} &= [0.5 C_L \rho (V_{X,R}^2 + V_{Y,R}^2) A_{RUD} \cos(\gamma_R \beta_R) + 0.5 C_D \rho (V_{X,R}^2 + V_{Y,R}^2) \\ &\quad A_{RUD} \sin(\gamma_R \beta_R)] (1+a_H) K_{Rud} = -Y_{Rud} Z_R M_{Rud} = -X_{Rud} Z_R N_{Rud} = Y_{Rud} X_R\end{aligned}\quad (15)$$

$$\begin{aligned}C_L &= \frac{2\pi \Lambda_{eff} (\Lambda_{eff} + 1) \sin(\alpha)}{(\Lambda_{eff} + 2)^2} \lambda, \\ \text{where } \Lambda_{eff} &= \left(2 - 0.016 \left| \frac{\delta}{\pi} \right| \right) \Lambda_{geom}\end{aligned}\quad (16)$$

$$C_D = \frac{1.1 C_L^2}{\pi \Lambda_{eff}} + C_{D0}$$

In the above Eqs. 15 and 16 the stall of the rudder was assumed to be 30° and λ presents a lift reduction factor in way of the slip-stream radius defined according to (Söding, 1982) and (Brix, 1993) as:

$$\lambda = \left(\frac{V_A}{V_{corr}} \right)^f, \text{ where } f = 2 \left(\frac{2}{2 + \frac{0.886(r+\Delta r)}{C_{rud}}} \right)^8 \quad (17)$$

The effects of vortical flow on the rudder were neglected. The influence of the hull ahead of the rudder was included in the rudder force as a factor of the order $(1 + a_H)$. This represents the increase of the lateral force due to the presence of the hull above the rudder root (Söding, 1982):

$$a_H = \frac{1}{1 + \left(\frac{4.9(x_P - x_R)}{T} + \frac{3C_{rud}}{T} \right)^2} \quad (18)$$

The propeller flow velocity forms an angle β_R (see Fig. 2). Therefore, the total angle of attack α at the rudder, including the rudder deflection δ was defined as:

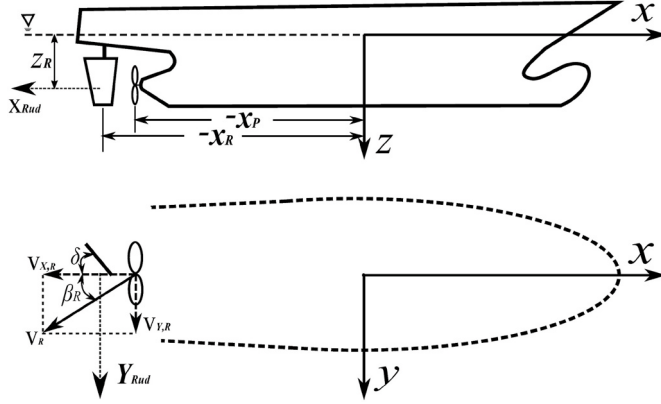


Fig. 2. Representation of the rudder forces and flow velocity at the rudder plane.

$$\beta_R = \left(\tan^{-1} \left(\frac{V_{Y,R}}{V_{X,R}} \right) \right) \quad (19)$$

$$\alpha = \delta + \gamma_R \beta_R$$

The above is based on the description of the rudder angle as illustrated in Fig. 2; γ_R is the flow straightening coefficient depending on the hull form and turning motion of the ship (Yasukawa and Yoshimura, 2015). This idealization is of relevance for a scenario whereby a ship is maneuvering and the flow passing through the hull of the ship reduces the angle of attack on the rudder (Liu and Hekkenberg, 2017; Molland and Turnock, 2007).

The flow straightening coefficient for a single screw and single propeller configuration was then defined according to Lee and Shin (1998) as:

$$\gamma_R = -\frac{1.20501 C_B B}{L} + 0.7391, \beta_R \leq 0 \quad (20)$$

$$\gamma_R = 2.7236 \frac{C_B B}{L} + 0.021, \beta_R > 0$$

3.3.2. Twin Propeller Twin Rudder (TPTR) configuration

The TPTR configuration assumed that both propellers have similar

design characteristics and therefore hydrodynamic flow effects differ only in terms of flow-straightening coefficients. Accordingly, the twin-screw/rudder flow straightening coefficient was defined as:

$$\gamma_{R(p,s)} = -\frac{1.20501 C_B B}{L} + 0.7391, \beta_R \leq 0 \quad (21)$$

$$\gamma_{R(p,s)} = 2.7236 \frac{C_B B}{L} + 0.021, \beta_R > 0$$

3.4. Hull hydrodynamic in-plane forces

As per (Taimuri et al., 2019) the in plane hull forces acting on an SPSR and TPTR configuration can be defined as:

$$X'_{Hull} = X'_{vv} v'^2 + X'_{vr} v' r' + X'_{rr} r'^2 + X'_{vrv} v'^4$$

$$Y'_{Hull} = Y'_{vv} v' + Y'_{vr} r' + Y'_{vv} v'^3 + Y'_{vv} v'^2 r' + Y'_{vrr} v'^2 r'^2 + Y'_{rrr} r'^3 \quad (22)$$

$$N'_{Hull} = N'_{vv} v' + N'_{vvr} v'^2 r' + N'_{vvv} v'^3 + N'_{rr} r' + N'_{vrr} v'^2 r'^2 + N'_{rrr} r'^3$$

$$K'_{Hull} = -Y'_{Hull}(0.5T)$$

In Eq. (22) the external sway hydrodynamic damping term (Y_{Hull}) contributes to roll damping (K_{Hull}). The point of the lateral hull force (Y_{Hull}) acts at some distance in between the still water line and the keel of the ship. This vertical distance can be calculated by a static drift test (Kim et al., 2007) or from charts available in literature (e.g. Hirano and Takashina, 1980). Along these lines, “0.5T” may be considered acceptable estimate of effect of external sway force on roll moment. It is noted that the model does not account for coupling between yaw and roll motions. This is because during grounding the change in wetted surface area and flow over non-symmetrical part of the hull are minimal and hence maneuvering is not affected by the small amplitudes of heave, roll and pitch. Notwithstanding, to further justify this choice two different cases of calm water simulations at high speed deep waters and at low speed shallow waters were considered with yaw-roll coupled hydrodynamic coefficients as per (Hirano and Takashina, 1980). In both cases time histories of motion are identical (see Fig. 3). At low speed and shallow turning circle trajectories are practically the same (see Fig. 3(a)) and at higher speed and deep waters some rather marginal differences become evident (see Fig. 3(b)).

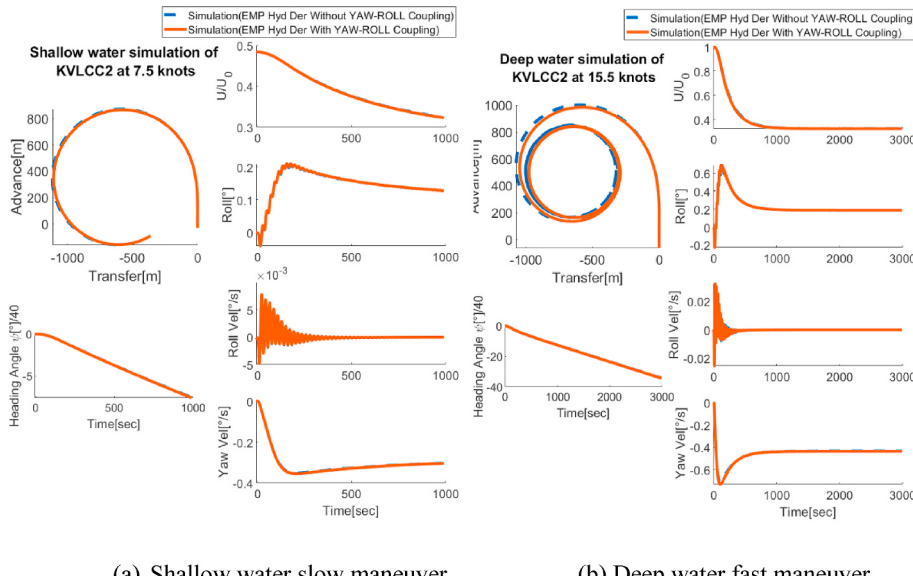


Fig. 3. Linear estimation of roll damping in different operational conditions.

- (a) Shallow water slow maneuver
- (b) Deep water fast maneuver

The non-dimensional hull forces and velocities for a ship progressing with instantaneous velocity U were defined as:

$$\begin{aligned} X'_{Hull} &= \frac{X_{Hull}}{0.5\rho L_{pp}^2 U^2} \\ Y'_{Hull} &= \frac{Y_{Hull}}{0.5\rho L_{pp}^2 U^2} \\ N'_{Hull} &= \frac{N_{Hull}}{0.5\rho L_{pp}^3 U^2} \\ v' &= \frac{v}{U} \\ r' &= \frac{rL_{pp}}{U} \end{aligned} \quad (23)$$

The maneuvering hydrodynamic derivatives can be defined by CFD simulations, regression-based semi-empirical equations or model tests. The semi-empirical formulas presented in Table 6 (Appendix B) summarize the hydrodynamic coefficients for an SPSR vessel. The 6-DoF surge, sway, heave, roll, pitch and yaw added mass approximations are summarized in (Appendix A, Table 5). Surge, sway and yaw added masses were defined according to (Brix, 1993; Clarke et al., 1982) and roll, pitch and heave added masses were defined from the strip theory of (Frank, 1967; Journée, 1992).

3.5. Reference technique for the evaluation of maneuvering hull coefficients

The empirical formulae presented in Table 6 (Appendix B), are for a single-screw vessel only. CFD or PMM based hydrodynamic coefficients of a TPTR ship could be used. However, CFD simulations or PMM tests are expensive. Thus, a novel reference technique that may be applicable to

either SPSR or TPTR vessels was derived for the improved prediction of hull external forces. The method assumes that the changes in the hydrodynamic coefficients may be attributed to changes in the main particulars of a TPTR ship and are of the same order as for equivalent SPSR ships. The procedure is illustrated in Fig. 4, where as an example the hydrodynamic coefficients of a reference TPTR vessel known from PMM tests are defined as " C_{true}^{ref} ". The coefficients calculated using the combination of semi-empirical formulations presented in Appendix B are defined as " C_{approx}^{ref} " and the corresponding coefficients for a new-build TPTR vessel are defined as " C_{approx}^{nb} "; " $C_{estimate}^{nb}$ " is evaluated once a sufficient correlation of C_{true}^{ref} with C_{approx}^{nb} is established according to the formulae:

$$C_{estimate}^{nb} = \left(\frac{C_{true}^{ref}}{C_{approx}^{ref}} \right) C_{approx}^{nb} \quad (24)$$

The linear reference technique proposed is essentially a model calibration technique. The theoretical basis of this technique relies on the use of a correction factor namely $C_{true}^{ref}/C_{approx}^{ref}$ that (obviously) makes use of the results (model test C_{true}^{ref} - known values from experiments and C_{approx}^{ref} empirical formula) of the reference ship. This is done separately for each hydrodynamic coefficient producing a set of correction factors. These correction factors are then used to correct the new vessel (C_{approx}^{nb}) hydrodynamic derivatives originating from the empirical formulas (C_{approx}^{nb}) for the new ship Eq. (24) (manuscript). The idea is to reduce the uncertainties of hydrodynamic coefficients of a twin-screw vessel when utilizing single screw semi-empirical hydrodynamic coefficients. Similar sort of approach is used for converting deep water hydrodynamic derivatives to shallow water by means of a correction factor for linear and higher order hydrodynamic coefficients (Kijima et al., 1990; Vantorre, 2001).

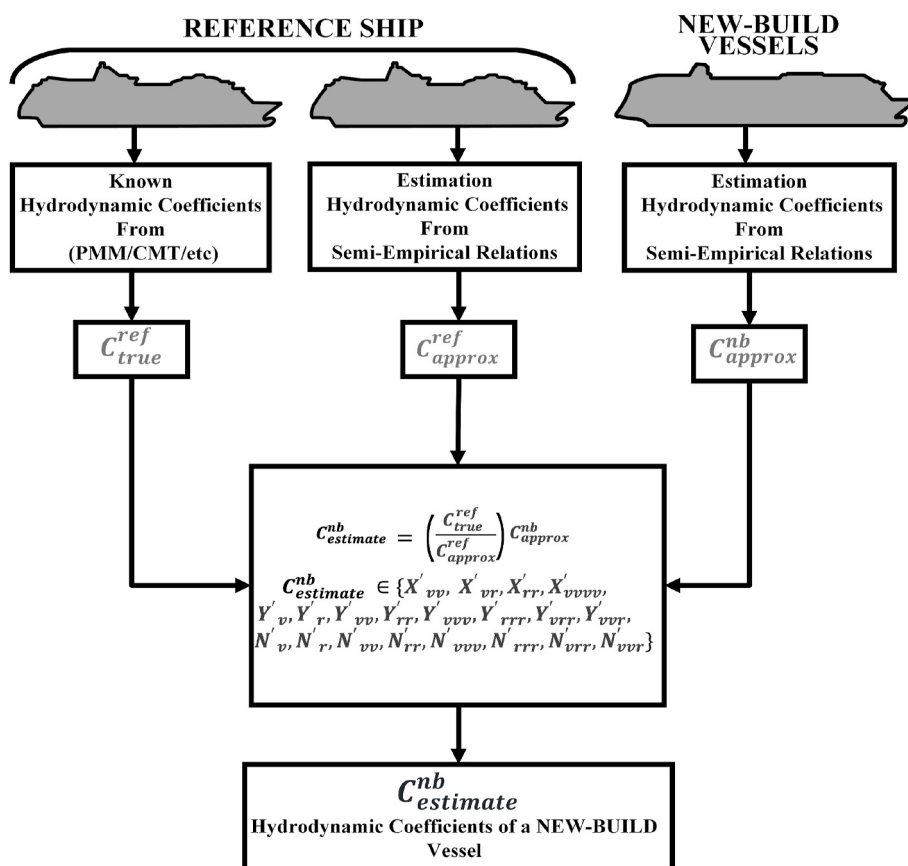


Fig. 4. Reference technique for the estimation of hydrodynamic coefficients of TPTR.

3.6. Shallow water effects

Shallow water corrections accounted for viscous resistance as per Raven (2016):

$$\frac{C_v}{C_{v_{deep}}} = 1 + 0.57 \left(\frac{T}{H} \right)^{1.79} \quad \text{for } \frac{T}{H} < 0.5 \quad (25)$$

where, $C_{v_{deep}}$ was calculated as per ITTC (2017b). The increase of added masses due to shallow water effects and surge damping were defined as per Ankudinov et al. (1990). Sway and yaw linear, higher-order and coupled hydrodynamic derivatives were approximated using a combination of Kijima et al. (1990b) and Ankudinov et al. (1990) formulations (see Table 7, Appendix C). Eq. (26), shows the implementation of the wake fraction, thrust deduction and flow-straightening coefficient in shallow waters according to Amin and Hasegawa (2010).

$$X_{SW} = FX_{SW}\alpha_T \left(\frac{0.87}{C_B} \right)^{1+4\sqrt{F_n}} \sec \alpha_{WL}, \text{ if } \left\{ \frac{\pi}{2} < \alpha < \frac{3\pi}{2} \right\}, \text{ else} \quad (32)$$

$$X_{SW} = FX_{SW}\alpha_T$$

$$Y_{SW} = FY_{SW}\alpha_T \quad (33)$$

$$N_{SW} = MN_{SW}\alpha_T \quad (34)$$

$$\alpha_T = 1 - e^{-2kT}, \text{ } k \text{ is the wave number} \quad (35)$$

$$w_{Shallow} = \left(1 + \left(-4.932 + 0.6425 \frac{C_B L}{T} - 0.0165 \left(\frac{C_B L}{T} \right)^2 \right) (T_H)^{1.655} \right) * w_{deep} \frac{1-t_{Shallow}}{1-t_{deep}} = 1 + \left(\left(29.495 D_0 - 14.089 \frac{C_B L}{B} + 1.6486 \left(\frac{C_B L}{B} \right)^2 \right) \left(\frac{1}{250} - \frac{7}{200} T_H - \frac{13}{125} T_H^2 \right) \right) \frac{\gamma_{R_{Shallow}}}{\gamma_{R_{Deep}}} = 1 + \left(\left(-\frac{5129}{500} + 178.207 \frac{C_B B}{L} - \frac{2745}{4} \left(\frac{C_B B}{L} \right)^2 \right) \left(-\frac{1927}{500} + \frac{2733}{200} T_H - \frac{2617}{250} (T_H)^2 \right) \right); \text{ for } T_H \leq \left(-0.332 \frac{T}{B} + 0.581 \right), \\ \gamma_{R_{Shallow}} = 1 + \left(-\frac{541}{4} + 2432.95 \frac{C_B B}{L} - 10137.7 \left(\frac{C_B B}{L} \right)^2 \right) (T_H^{4.81}) \quad (26)$$

3.7. Short waves

A model that considers only short waves ($\frac{\lambda}{L_{PP}} \leq 0.5$) was implemented. Added resistance was assumed proportional to the square of wave amplitude (Faltinsen, 1990). The second-order mean short wave forces due to small wavelength were defined according to (Sakamoto and Baba, 1986) and the coordinate system of Fig. 5 as:

$$F_i = 0.5\rho g \zeta_a^2 \int_{L_1} \left\{ \cos^2(\alpha) + \frac{2\omega_0 U}{g} [-\cos\beta_w - \cos(\theta)\sin(\alpha)] \right\} n_i dl \quad (27)$$

The surge, sway forces and yaw moment were defined as:

$$FX_{SW} = 0.5\rho g \zeta_a^2 \sum_{i=1}^{n-1} \left\{ \cos^2 \alpha_i + \frac{2\omega_0 U}{g} [-N_{WX} - N_Y \sin \alpha_i] \right\} N_X dl_i \quad (28)$$

$$FY_{SW} = 0.5\rho g \zeta_a^2 \sum_{i=1}^{n-1} \left\{ \cos^2 \alpha_i + \frac{2\omega_0 U}{g} [-N_{WX} - N_Y \sin \alpha_i] \right\} N_Y dl_i \quad (29)$$

$$MN_{SW} = 0.5\rho g \zeta_a^2 \sum_{i=1}^{n-1} \left\{ \cos^2 \alpha_i + \frac{2\omega_0 U}{g} [-N_{WX} - N_Y \sin \alpha_i] \right\} (x_0 N_Y - y_0 N_X) dl_i \quad (30)$$

$$\alpha = \beta_w - \psi - \beta \quad (31)$$

Details on the numerical integration are shown in Appendix D, where the integration is performed along the non-shadow region of the hull waterline. For a sailing ship added resistance in short waves is affected by the draft of the ship described in (Liu et al., 2016). Hence, the draft and speed correction factor were incorporated in the equation of added resistance in short waves as:

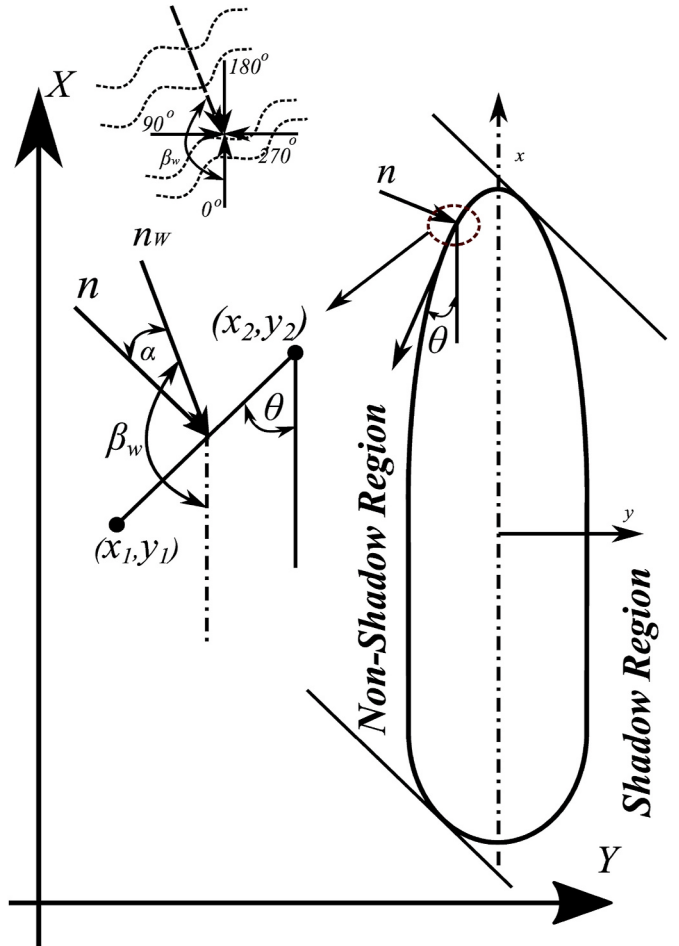


Fig. 5. Direction and slope of short waves in relation to the hull waterline profile.

4. Maneuvering simulations

4.1. General approach

The method developed is summarized in Fig. 6. The general particulars of the hull, resistance curve, rudder and propeller details were the assumed input. Hydrodynamic derivatives were then derived from semi-empirical formulations, model tests, CFD and/or their combinations. When

considering shallow waters there is an increase in ship resistance, added masses and damping, incorporated in the model (Taimuri et al., 2019). To maintain the rapidness of the method the influence of short waves was precomputed by numerically integrating the waterline and adding as input a response surface accounting for wave heading, ship speed and associated hydrodynamic actions (Chroni et al., 2015; Papanikolaou et al., 2016). A Runge-Kutta solver of the 4th order was used to solve the differential equations (Matusiak, 2017). Since motions represented by Eq. (2), are

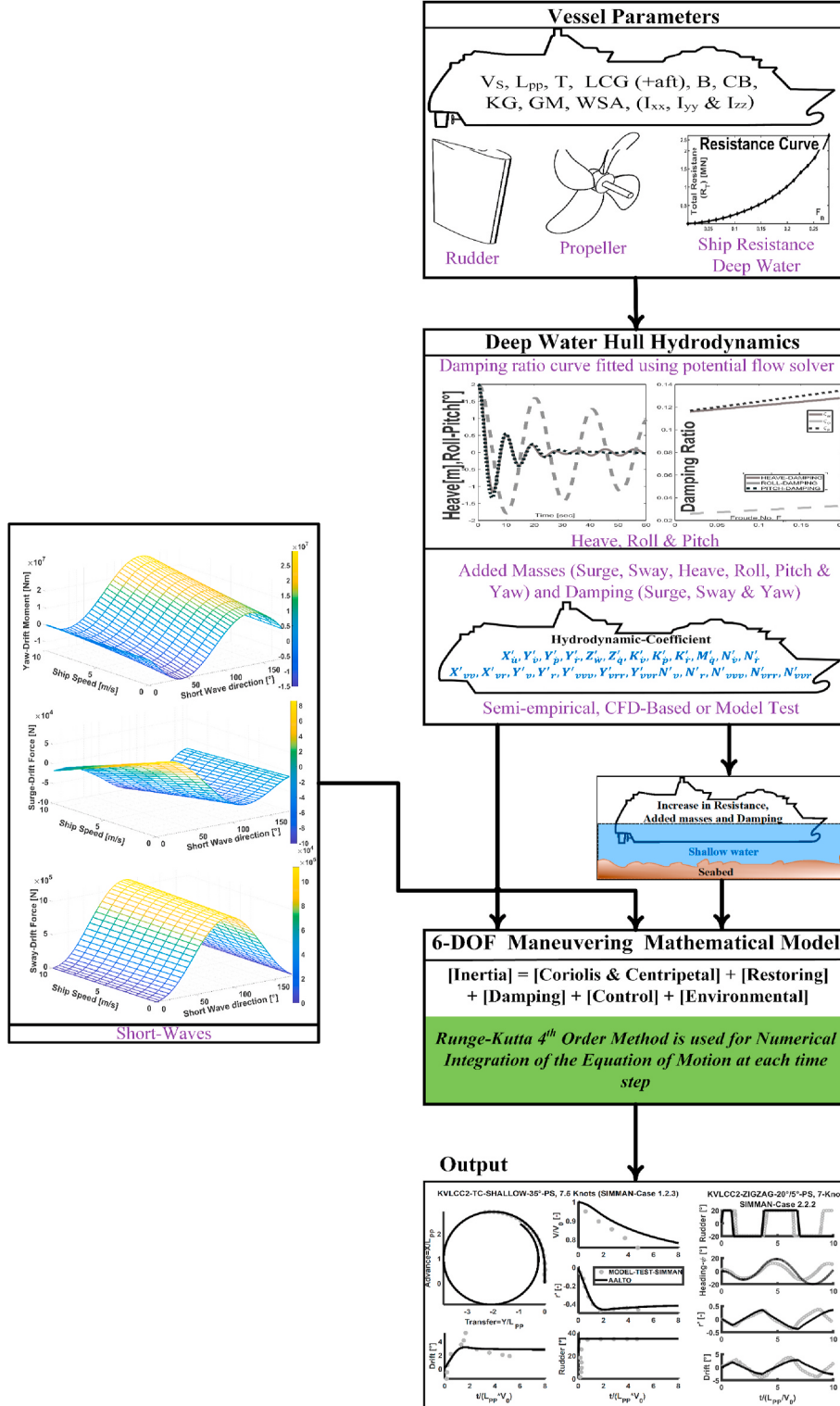


Fig. 6. Procedure and approach for simulating 6-DOF ship motions.

coupled through acceleration terms, the equations were first de-coupled numerically and in turn accelerations were integrated into velocities considering input from each time step. At the same time step velocities were integrated into position vectors using Eq. (1). The differential ordinary equation used to evaluate the rudder angle set by the autopilot controller was defined as Eq. (36), (Matusiak, 2017).

$$\dot{\delta} = \text{sgn}(\delta_T - \delta)\omega_\delta \quad (36)$$

4.2. Simulation cases

Ship general particulars are summarized in Table 1. The method was tested and validated against experimental records for DTC (Chillcce and el Moctar, 2018); KVLCC2 and ONRT (SIMMAN, 2020) and key data made available from a shipyard for FSB.

DTC and KVLCC2 resistances were obtained from the benchmark study of (Sprenger et al., 2015) and (Adolfo Marón, 2016) respectively. The (Holtrop and Mennen, 1982) method was utilized to obtain the resistance of ONRT and FSB ships (see Fig. 7). The open water propeller characteristics curve for DTC were defined as per (Sprenger et al., 2015) and for KVLCC2 according to (Stern et al., 2011). Based on propeller parameters the K-T curves of FSB were estimated based on the Wageningen B-propeller series (Bernitsas et al., 1981) and for the ONRT propeller characteristics were gathered from (SIMMAN, 2020). A summary of all propeller parameters is given in Table 2. The Rudder details of the ships are summarized in Table 3.

Table 1
Ship general particulars.

Vessels	DTC	KVLCC2	ONRT	FSB
Ship Class	<i>Container</i>	<i>Tanker</i>	<i>Naval</i>	<i>Passenger</i>
Propulsion	<i>SPSR</i>	<i>SPSR</i>	<i>TPTR</i>	<i>TPTR</i>
Source	Sprenger et al. (2017)	SIMMAN (2020)	Luhmann (2009)	
$L_{pp}[m]$	355	320	154	216.8
$B[m]$	51	58	18.78	32.2
$T[m]$	14.5	20.8	5.494	7.2
$C_B[-]$	0.661	0.8098	0.535	0.661
$S_w[m^2]$	22032	27194	3592	7822
$x_G + fwd [m]$	3.4	11.136	-2.5256	-8.8
$GM[m]$	5.1	5.71	2.068	2.6299
$KG[m]$	19.8	18.56	7.6384	15.18
$r_{xx}[m]$	20.3	23.2	8.335	14.17
$r_{yy}[m]$	87.3	80	37.884	54.2
$r_{zz}[m]$	87.4	80	37.884	54.2

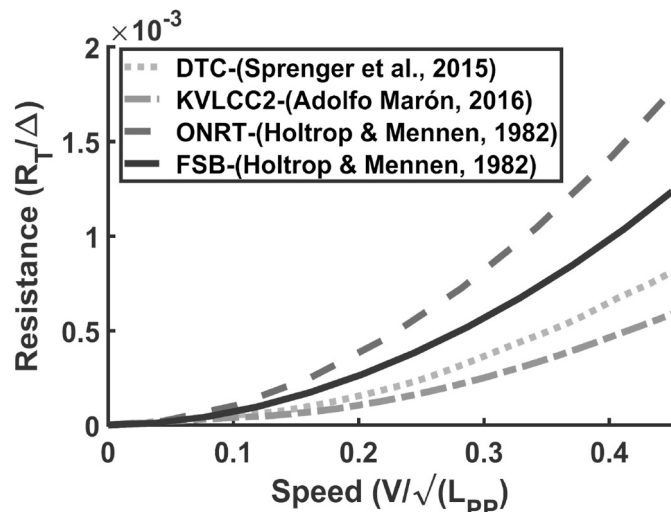


Fig. 7. Resistance curve of selected vessels.

Table 2
Propeller details and characteristic curves.

Vessels	DTC	KVLCC2	ONRT	FSB
Source	Chillcce and el Moctar (2018)	SIMMAN (2020)		Shipyard
$D[m]$	8.911	9.86	5.2165	5.2
$P/D (0.7R)$	0.959	0.721	—	1.167
A_e/A_0	0.8	0.431	—	0.936
Z	5	4	4	5
N_p	1	1	2	2
$x_p[m]$	-158.7	-153.5	-70	-104.2
k_{T0}	0.5122	0.3243	0.6426	0.583
k_{T1}	-0.424	-0.222	-0.28965	-0.23
k_{T2}	-0.0882	-0.148	-0.0865	-0.274

Table 3
Rudder specification.

	DTC	KVLCC2	ONRT	FSB
$S_R[m^2]$	255	273.3	57.278	40
$A_R[m^2]$	127.5	136.7	28.278	20
$A_{Rmov}[m^2]$	95.1	112.5	24.31	19.7
A_R	1.75	1.826	1.2	1.59
$x_R[m]$	-170.7	161.5	-74.305	-108.4
$z_R[m]$	5.05	6.5	2.85	4.3
<i>Rate of turn</i> [°/s]	2.25	2.34	5	5

4.3. Selection of hydrodynamic coefficients

Hydrodynamic coefficients were evaluated using the empirical formulation from the model test data of different ships given by (Clarke et al., 1982; Inoue et al., 1981; Khattab, 1984; Kijima et al., 1990a; Lee and Shin, 1998; Norrbin, 1970; Yoshimura and Masumoto, 2011) and are presented in Table 6, Appendix B. For both DTC and KVLCC2 Eq. (22) was used. Table 4 summarizes all hydrodynamic coefficients. The deep water semi-empirical formulae used for DTC are summarized in Table 6 in Appendix B. For deep waters KVLCC2 runs utilized model test hydrodynamic derivatives based on CMT measurements (Aksu and Köse, 2017) and semi-empirical hydrodynamic coefficients (see Appendix B). For shallow waters derivatives were selected from CFD (Mucha, 2017) and semi-empirical hydrodynamic coefficients (see Appendix C). The reference technique makes use of similar hull form and comparable control devices (see Fig. 4). A twin screw David Taylor model basin surface combatant (DTMB-5415) was used as reference ship for ONRT with hydrodynamic coefficients based on the PMM tests of (Yoon, 2009) as reported in (Sukas et al., 2019b). The hydrodynamic coefficient of a twin screw ferry with a bow thruster were chosen for FSB as presented in (Yasukawa and Hirata, 2013) (see Table 4).

4.4. Verification of heave, roll and pitch for the intended use

The objective of the verification process was to qualify that a linear undamped dynamic response caused by a step-wise excitation is twice the stationary response (Matusiak, 2000; Thorby, 2008). Accordingly, heave, pitch and roll motion responses were evaluated by dynamically heaving, heeling and trimming the vessel. Step forces were applied to the ship separately and then dynamic displacement and rotation were observed before the system converges to steady-state. Fig. 8, illustrates the dynamic response to an impulse, for the case of KVLCC2. The maximum heave, roll and pitch responses due to step loading were quantified as 1.97, 2.0 and 1.975 times the steady-state response amplitude respectively. In turning circle tests steady motion may be achieved after some time of the rudder execution, where the vessel path

Table 4
Hull hydrodynamic derivatives.

Vessels	KVLCC2		KVLCC2		DTC	DTMB-5415	ONRT	FERRY	FSB
Condition Source	Deep Aksu and Köse (2017)	Shallow Mucha (2017)	Deep Semi-empirical Appendix B	Shallow Appendix C	Deep Semi-empirical Appendix B	Reference Vessel (Yoon, 2009) as reported in (Sukas et al., 2019b)	Deep Reference Technique	Reference Vessel Yasukawa and Hirata (2013)	Deep Reference Technique
X'_{rr}	-0.003 0	-0.145 0.002	-0.00073 -0.00108	-0.0045 -0.0028	-0.0029 -0.0009	-0.00662 -0.00722	-0.00562 -0.00528	-0.00467 -0.00163	-0.00294 -0.00128
X'_{vvv}	0.001	0	-0.00084	-0.0024	0.0001	-0.00119	-0.00157	0	0
X'_{vvv}	0.053	0	0.00777	0.0482	0.0191	0	0	0.01745	0.01127
Y'_v	-0.02	-0.093	-0.02526	-0.1064	-0.0101	-0.01282	-0.00925	-0.01239	-0.00914
Y'_r	0.005	0.004	0.00494	0.0077	0.0019	0.00404	0.00255	0.00225	0.00097
Y'_{vv}	-0.103	-2.012	-0.04142	-0.2569	-0.0598	-0.08426	-0.07173	-0.08521	-0.05022
Y'_{vv}	0	0.02	-0.00047	-0.0014	0.0019	-0.00196	-0.00209	0	0
Y'_{vv}	-0.025	-0.129	-0.02638	-0.1636	-0.0235	-0.08748	-0.06162	0	0
Y'_{vv}	0.024	0.082	-0.01393	-0.0864	-0.0151	-0.0815	-0.0689	0.02052	0.01561
N'_v	-0.009	-0.034	-0.00871	-0.0389	-0.0031	-0.00722	-0.00475	-0.00361	-0.00211
N'_r	-0.003	-0.003	-0.00305	-0.003	-0.0013	-0.00213	-0.00133	-0.00241	-0.00119
N'_{vv}	-0.002	-0.034	-0.00124	-0.0077	-0.0163	-0.01886	-0.0142	-0.01012	-0.00168
N'_{vv}	-0.001	-0.01	-0.00125	-0.0037	-0.0013	-0.00219	-0.00183	0	0
N'_{vv}	0.004	-0.013	0.00619	0.0223	0.0018	-0.02984	0.02185 ¹	0	0
N'_{vv}	-0.019	0.014	-0.00897	-0.0085	-0.0152	-0.01891	-0.01634	-0.03004	-0.01786

1 The sign of the coefficient (N_{vv}) of ONRT has been changed as the original sign gives the unrealistically small turn of the ship, which is by our opinion should be positive. This is also indicated by (Sakamoto et al., 2012) that the single run method and curve fitting method results in different sign of N_{vv} and Y_{vv} .

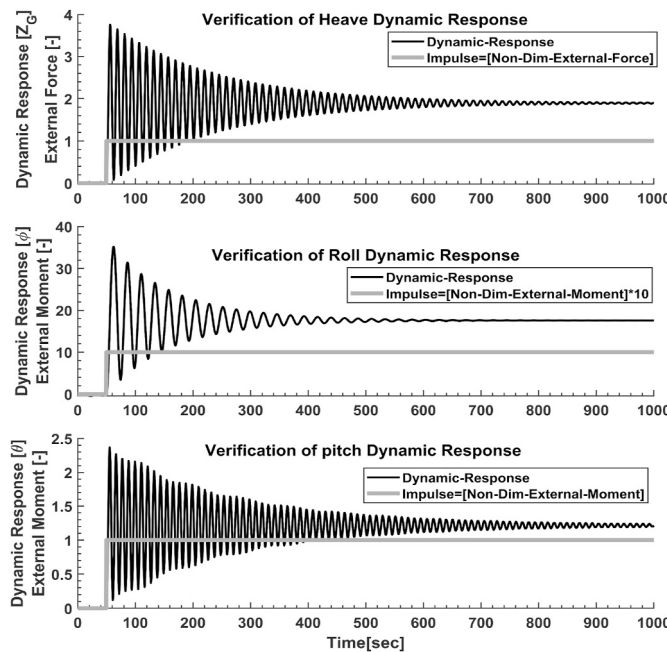


Fig. 8. Verification of heave, roll and pitch motions, where the dynamic response is almost twice the stationary value.

remains circular and this circular diameter and steady vessel speed are utilized to build the centrifugal force acting on the ship (see Eq. (37) and Matusiak, 2000). Such centrifugal force will contribute to an external moment ($M_{\varphi_{ext}}$), the external moment will be equal to the static righting moment (M_{st}) (see Eq. 38). Therefore, the analytical form of the heeling angle at a steady turn can be evaluated as:

$$F_{\varphi_{st}} = \rho \nabla \dot{\psi}^2 D_s / 2, \text{ where } \dot{\psi} = V_s / 0.5 D_s \quad (37)$$

$$M_{\varphi_{ext}} \approx \rho \nabla \dot{\psi} V_s (KG - 0.5T)$$

$$M_{st} = -\rho g \nabla GM_0 \varphi$$

$$M_{\varphi_{ext}} + M_{st} = 0$$

$$\rho \nabla \dot{\psi} V_s (KG - 0.5T) = \rho g \nabla GM_0 \varphi$$

$$\varphi \approx \dot{\psi} V_s \frac{(KG - 0.5T)}{g GM_0} \quad (38)$$

Simulation of the turning circle of KVLCC2 was performed at 35° rudder angle and 15.5 knots speed. Utilizing then Eqs. (37) and (38), the analytical steady yaw rate and heel angle were calculated as 0.51°/s and 0.259° respectively. Using simulations yaw rate and heel angles were estimated respectively as 0.5213°/s and 0.255°. These values show that there is a negligible difference of 2% percent between the numerical and analytical predictions.

5. Results and discussion

5.1. DTC and KVLCC2 SPSR ships

For DTC maneuvering simulations were compared to the work of (Chilcée and el Moctar, 2018) and results from EU FP7 SHOPERA project (<http://shopera.org/>). Fig. 9(a), illustrates good approximation of calm water turning circle trajectories. Minor fluctuations in the model test measurements appear possibly due to the reflection of the ship generated wave from the tank walls. Maneuvering in short waves seems to predict reasonable trajectories together with the translation motion only in the early stage of the turn. Drifting of the ship appears to deviate in head and following waves conditions (see Fig. 9(b,d)). Trajectories in beam seas follow the measured data. However, sway velocities are overpredicted in both head waves and following seas. This is reflected in the marginally imprecise drifting direction of the vessel's trajectory in head and following waves. Inconsistencies may appear due to differences in draft and speed correction factors or due to the fact that short waves assume vertical walls in way of the waterline and only reflection of the waves is considered. The influence of short waves on rudder and propeller forces are also neglected. In any case, the profile of the translational motions is well apprehended in the simulations. Numerical

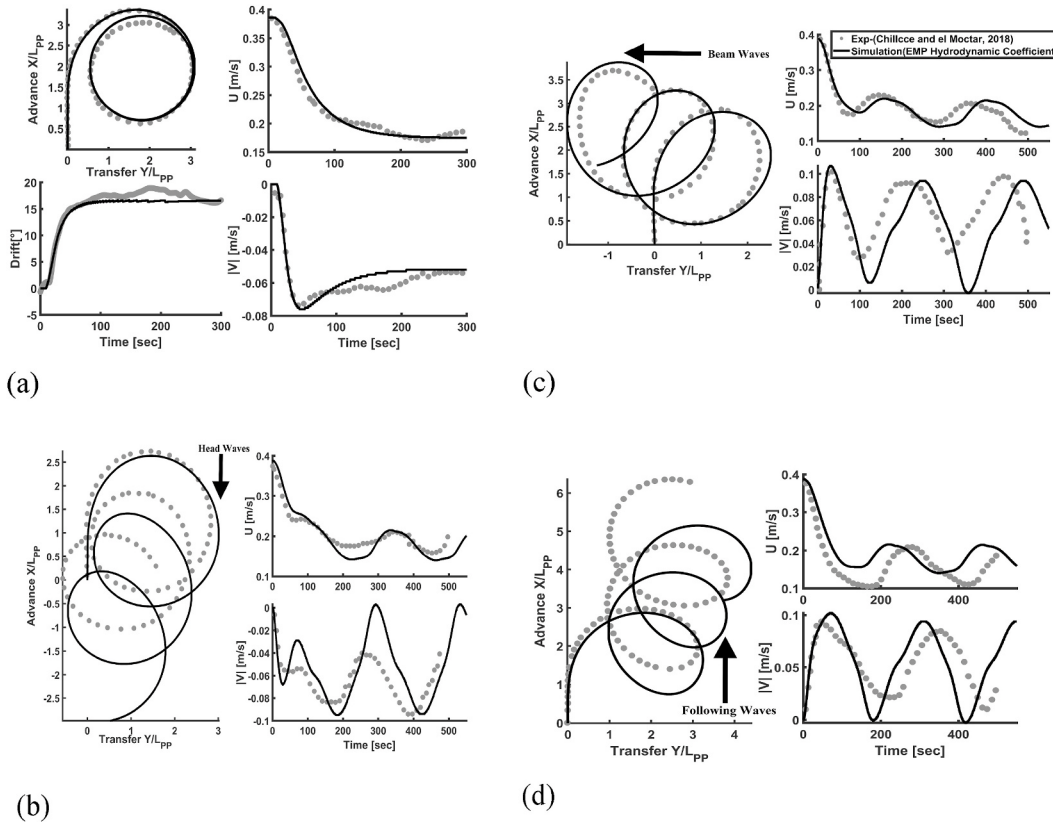


Fig. 9. DTC turning circle trajectories and translational motions for $\delta = 35^\circ$ (a) Calm waters; (b),(c),(d) represent simulations in head, regular and beam regular waves respectively for wave height 2m and frequency 0.592 rad/s.

simulations show that using semi-empirical based hydrodynamic coefficients (see Appendix B) may lead to correct estimation of initial trajectories and motions in deep calm waters and short waves. For KVLCC2 results were compared with the free-running model test

measurements of (SIMMAN, 2020). Fig. 10, illustrates the calm water simulations in deep-sea conditions. Comparisons were made against experimental values made available from (SIMMAN, 2020). The translation and rotation motions estimated from EMP simulations appear to

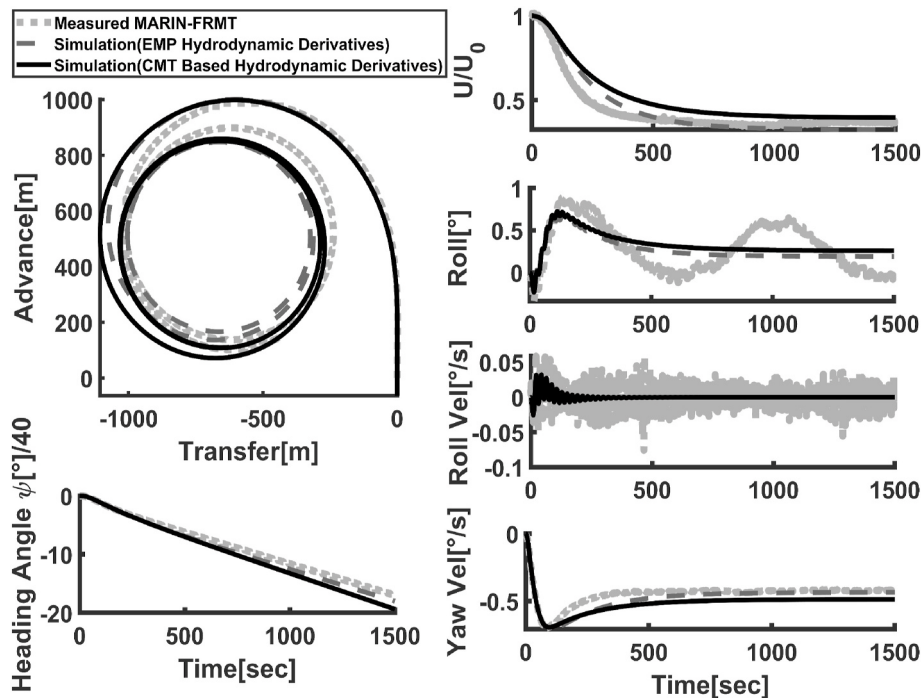


Fig. 10. KVLCC2 portside turn rudder angle of 35° , speed 15.5 knots. Calm water turning circle using EMP and CMT based hydrodynamic derivatives.

(a) $20^\circ/5^\circ$ zigzag turn 35° portside turning circle

correlate well in way of the steady state part of the model test measurements. Very little deviation was observed when CMT (Aksu and Köse, 2017) based hydrodynamic coefficients were used. The advance of the ship from simulations lies well within 2% of the measured data and therefore differences are numerically acceptable. It is possible that assumptions in defining the rudder forces (e.g. semi-empirical definition of the flow straightening coefficient) may have lead to larger drift angle predictions of the ship.

Fig. 11(a) and (b) illustrate the validation of 20°/5° zig-zag and 35° portside turning circle maneuvers in calm - shallow waters conditions respectively. Differences in turning circle trajectory are more significant when EMP instead of CFD hydrodynamic derivatives are used (see Fig. 11(b)). This is not the case for zig-zag test with rudder angle of 20° (Fig. 11(a)). Moreover, the zigzag test validates well with the initial heading and yaw rate until the reach of the ship (zero heading after first execute). Afterwards, results start deviating. The drift angle is underpredicted in comparison to the free-running model test (Fig. 11). Measured tests conducted in shallow waters for KVLCC2 at different

model tanks confirm these variations (Eloot et al., 2015). A validation of the differences pertaining to deep and shallow water maneuvering phenomena are shown in Fig. 12. Simulations for KVLCC2 based on empirical hydrodynamic coefficients, confirm that the model behavior follows the physics of deep and shallow water simulations (Vantorre et al., 2017). Whereas the tactical diameter and steady turn rate increase, irrespective to the trajectory the influence of sway motions and yaw rate remain small. The fact that a larger drift angle causes higher advance of the ship is related to the free under-hull flow effects.

5.2. ONRT and FSB TPTR ships

The maneuvering simulations and their validations presented in this section aim to demonstrate the reliability of the developed reference method (see Table 4 and Figs. 4 and 6) for TPTR vessels. ONRT trajectories and motions comparisons were made against (SIMMAN, 2020). Fig. 13, illustrates the calm water 35° portside turning circle simulation of ONRT. Excluding heave displacement and heave velocity, the

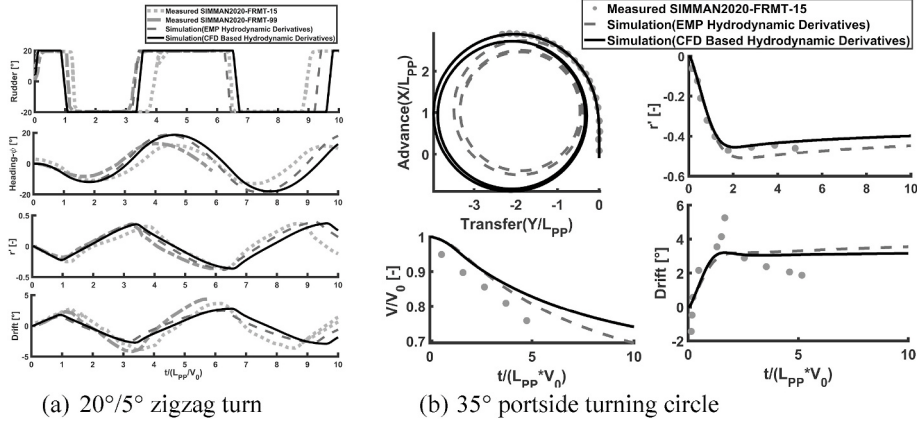


Fig. 11. KVLCC2 shallow water H/T = 1.2 at 7.5 knots, compared with two FRMT measurements.

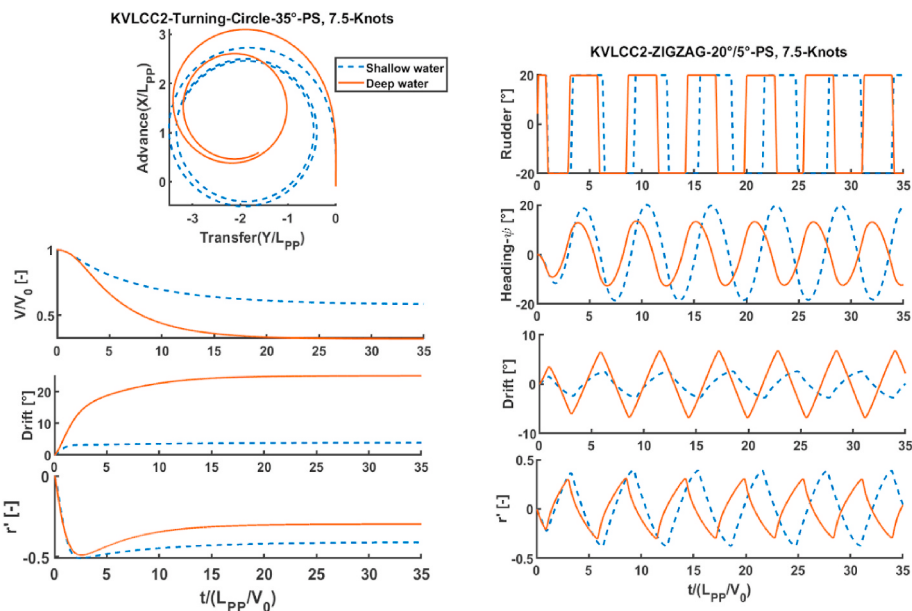


Fig. 12. Comparison of deep and shallow water simulation.

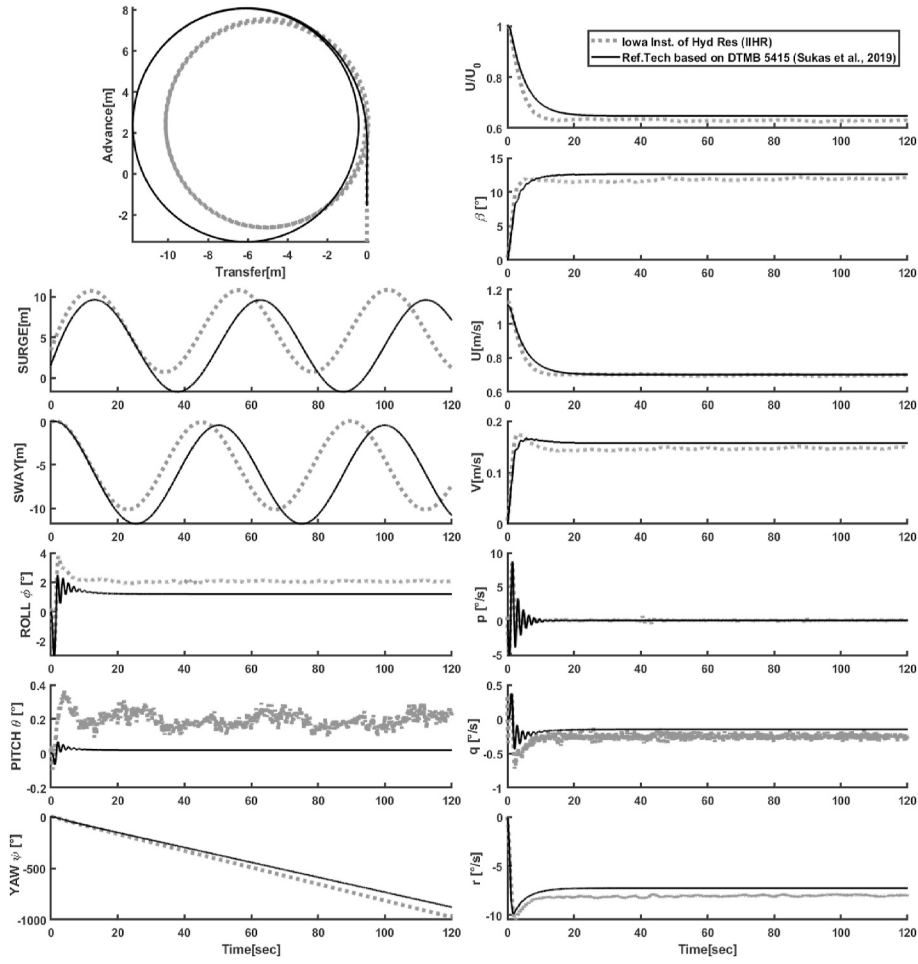


Fig. 13. ONRT Turning circle 35° portside, 15.1 knots. Track plus time histories of relevant motions.

remaining 5-DOF motions have been presented along the ship's track. The profile of all motions matches the trajectories from model test data. Advance of the ship is within 8% range of the measurement data. However, differences in numerical versus experimental surge and sway velocities and slower rate of change of ship heading angle results in 16% increase in ship transfer and tactical diameter. For the case of 20° zig-zag maneuver toward the starboard side shown in Fig. 14, reasonable trajectories and time histories of motions were obtained. The 1st and 2nd overshoot angles are within 15% of the free running model test. Notwithstanding, there is a slight decrease in the reach and period of the zig-zag maneuver (13% and 7% respectively). Other than pitch angular displacement all other translational and angular displacements and velocities, match almost perfectly at the initial phase of the turning maneuvers despite the small increase motion periods. The model does not take into account the roll induced pitch moment, which might explain the deviation in pitch behavior. For FSB calm water maneuvering simulation comparisons were based on numerical data provided by a shipyard. Fig. 15 (top) illustrates differences in the steady-state part of the turning circle maneuver. These discrepancies may relate to numerical simulation uncertainties. The simulation of the zig-zag maneuver shown in Fig. 15 (bottom) is quite satisfactory. A slight decrease of the surge velocity drop of the ship is observed in all cases. This ranges from

2% to 9% as compared to model experiments (see Figs. 13–15). The yaw rate from the model scale measurements is higher than computational results for the case of the turning circle trajectories (it varies between 11 and 20%). Additionally, a phase shift in yaw is noticed in zig-zag maneuver of ONRT.

Figs. 16 and 17 show the turning circle and zig-zag trajectory comparisons of hydrodynamic coefficients that have been empirically estimated using Eq. (22), Appendix B and Table 6, against those used in the reference technique for ONRT. When the empirical hydrodynamic coefficients for TPTP configuration ships are employed the yawing rate of the ship increases by 35%. For the FSB vessel turning circle the speed drop from empirical and reference techniques are almost equal (see Fig. 18 - top). This may be due to similar trends in increasing yaw rates. On the other hand, the trajectory obtained when the empirical formula is used is smaller. Although the speed drop matched well for the zig-zag maneuver of FSB (see Fig. 18 - bottom), amplitudes of motions are considerably larger than the ones simulated by the reference technique. In all cases only roll motion appears to match well against results when the empirical formulae is used.

As illustrated in Figs. 16–18, that semi-empirical hydrodynamic coefficients for a SPSR ship (see Table 6; Appendix B) is not the best choice for estimating maneuvering of a TPTP vessel. This is because it shows

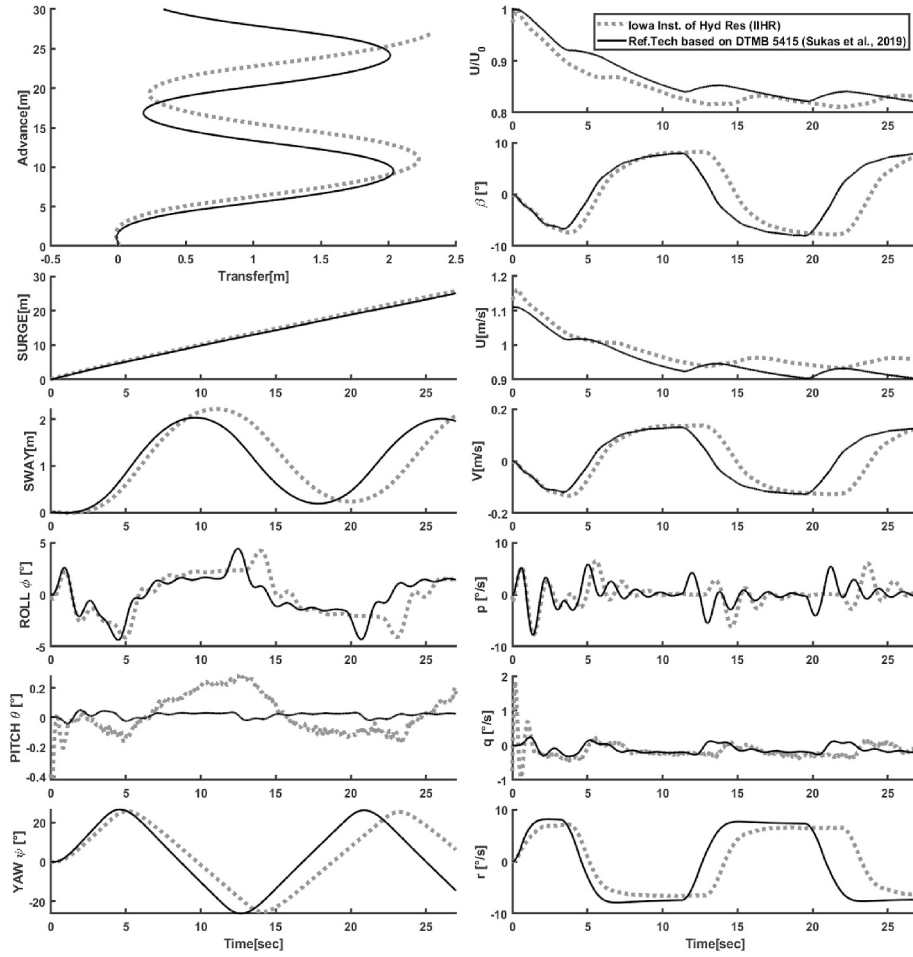


Fig. 14. ONRT zigzag maneuver 20° starboard side, 15.1 knots. Track plus time histories of relevant motions.

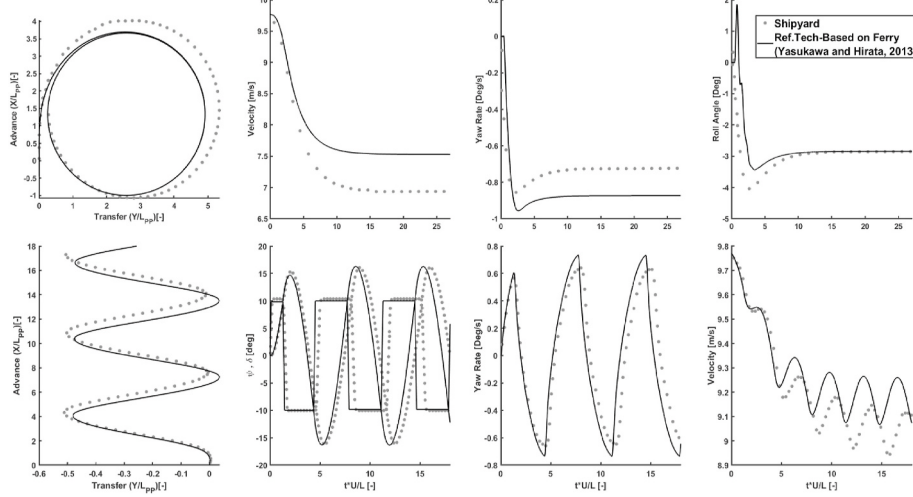


Fig. 15. FSB turning circle 15° starboard side (top), zigzag maneuver 10° portside (bottom). Track plus time histories of relevant motions. (19 knots).

poor performance in terms of evaluating ship trajectories and motion time histories. Therefore, the reference method as proposed above seems to give good results for ONRT and FSB, where the reference ship is a surface combatant for ONRT and a ferry with a bow thruster for FSB vessel. The key reasons of discrepancies may be attributed to the following:

- During PMM tests the model is towed at a constant speed. On the other hand, the mathematical model accounts for the instantaneous ship velocity and assumes that the velocity drop may be overcome by making hydrodynamic coefficients non-dimensional.
- For both ships resistances, wake fraction and thrust deduction are estimated from (Holtrop and Mennen, 1982) formulation. Similarly, flow straightening coefficients are semi-empirically calculated. One way to reduce certain level of uncertainties in the estimation of

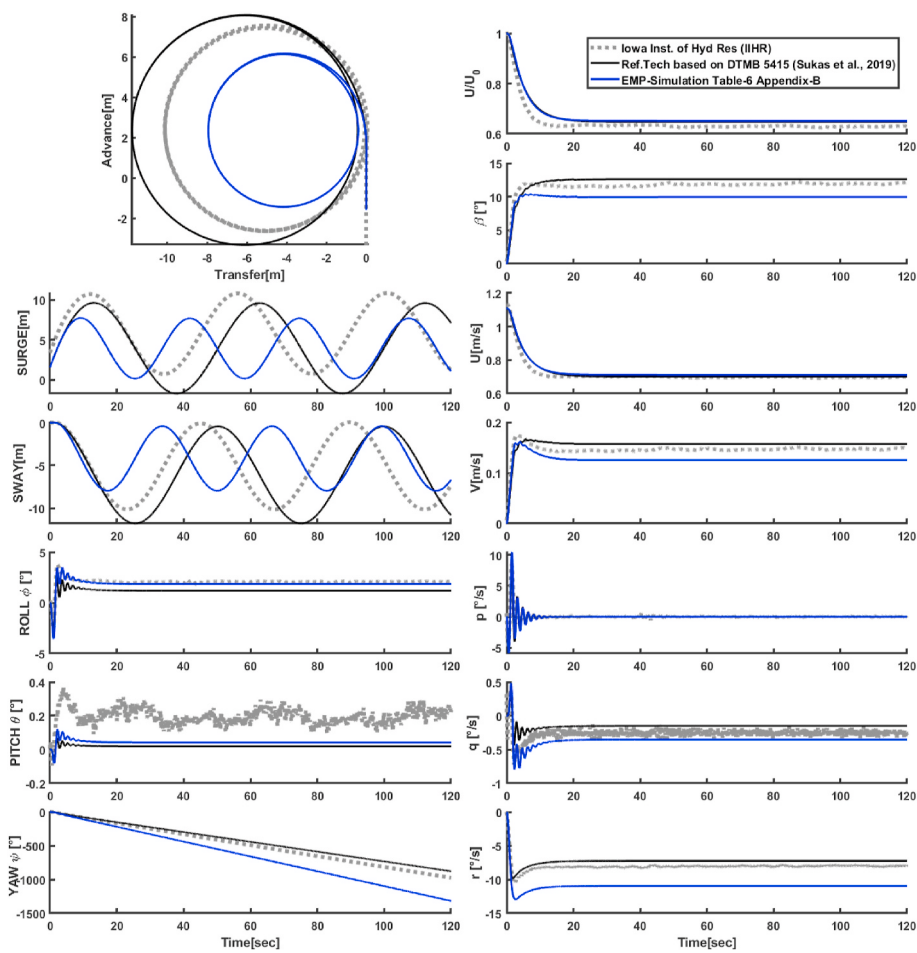


Fig. 16. ONRT turning circle test comparison. (empirical hydrodynamic coefficients against reference technique).

flow-straightening coefficient, wake fraction and thrust deduction factor is to implement the reference technique on these parameters obtained from similar kind of vessel. However, this approach lies beyond the scope of this publication.

- The sources of uncertainties in the model scale PMM test are transferred to the reference techniques. Thus, results also depend on how well the experiments are performed.

6. Conclusions

This paper presents a 6-DoF modular maneuvering model and reference technique that may be used for the rapid estimation of maneuvering trajectories and motion time histories of single or twin-screw propulsion ships. Results were validated against experiments available for zig-zag and turning cycle trajectories of vessels with different hull forms and propulsion configurations. It was demonstrated that by suitably combining existing semi-empirical formulations for the hull, rudder and propulsion hydrodynamics found in literature into a single formulation satisfactory prediction of maneuvering trajectories for SPSR ships of differing type can be obtained. Whereas experimental data for a broader range of ship designs were not available it is believed that the reference technique proposed provides reasonable maneuvering

predictions for TPTR ships with significantly different main particulars. It is therefore believed that the method and modelling approach presented could be used to simulate well ship dynamics. It is noted that whereas the model could also be combined with gusty winds, dynamic positioning or towing models, such applications are out of scope of this research that intends to better understand the influence of hydrodynamic actions on hard grounding induced dynamic response.

CRediT authorship contribution statement

Ghalib Taimuri: Methodology, Software, Validation, Formal analysis, Investigation, Data curation, Writing - review & editing. **Jerzy Matusiak:** Conceptualization, Writing - review & editing, Data curation. **Tommi Mikkola:** Conceptualization, Validation, Writing - review & editing, Supervision, Data curation. **Pentti Kujala:** Writing - review & editing. **Spyros Hirdaris:** Conceptualization, Validation, Writing - review & editing, Supervision, Funding acquisition, Project administration.

Declaration of competing interest

The authors declare that they have no known competing financial

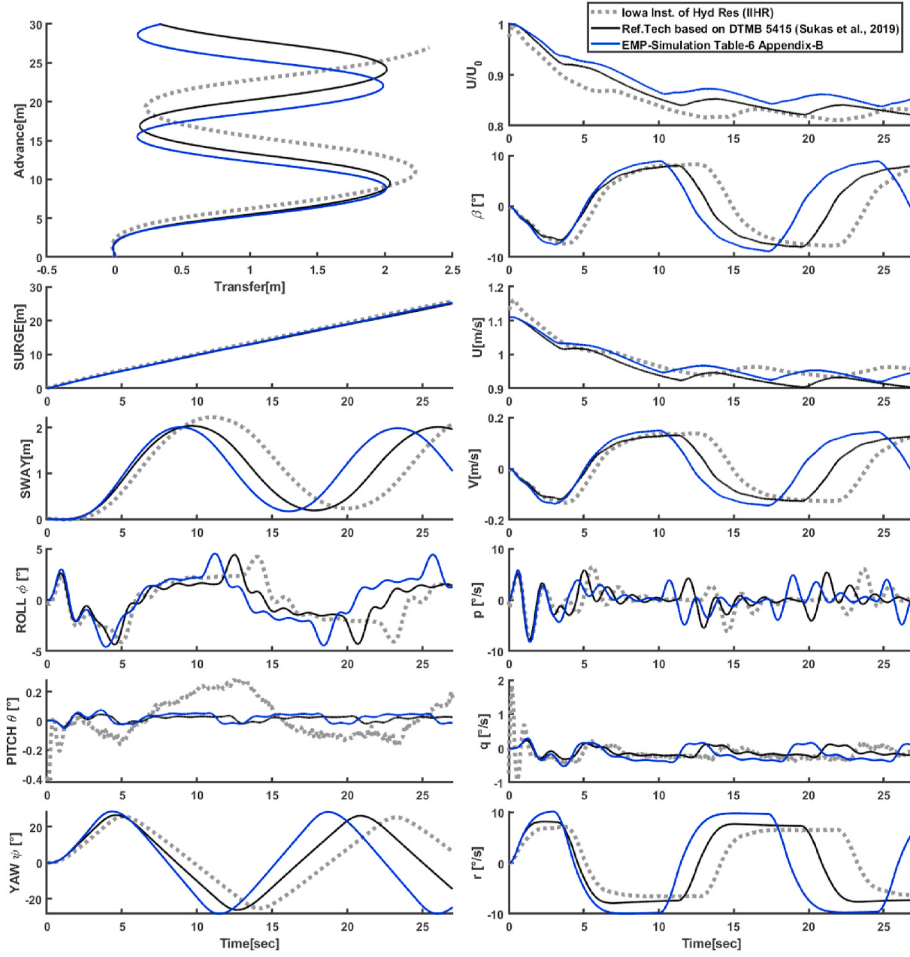


Fig. 17. ONRT zigzag test comparison. (empirical hydrodynamic coefficients against reference technique).

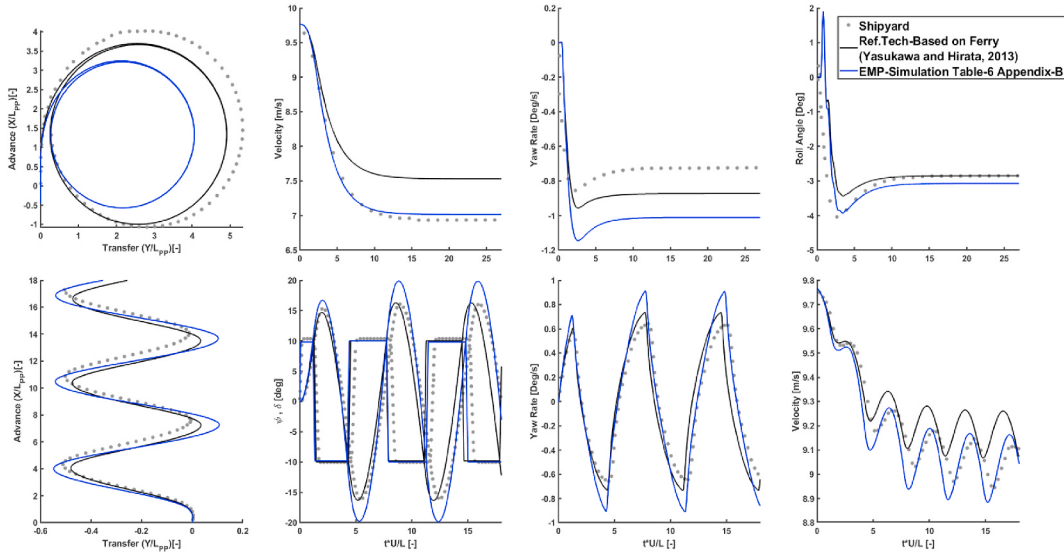


Fig. 18. FSB Turning circle (Top) and zigzag maneuver (bottom). (empirical hydrodynamic coefficients against reference technique).

interests or personal relationships that could have appeared to influence the work reported in this paper.

Acknowledgement

The research presented in the paper has been carried out under EU

Horizon 2020 project FLooding Accident REsponse (FLARE – Contract No. 814753). Special thanks of appreciation are conveyed to Meyer Turku and SIMMAN, 2020 for making available benchmark data for the presented maneuvering simulations. Spyros Hirdaris acknowledges financial support from the Academy of Finland University competitive funding award (SA Profi 2-T20404). Spyros Hirdaris and Ghalib Taimuri

acknowledge funding from Finnish Maritime Foundation - Merenkulun Säätiö (Award no.: 202000008).

Appendix A

Table 5
Approximation of Added masses.

$X_u = \frac{\partial X}{\partial u}$	$\frac{m}{\pi\sqrt{\frac{L^3}{\nabla} - 14}}$ Brix (1993)
$Y_v = \frac{\partial Y}{\partial v}$	$0.5\rho L^3 \left(-\pi \left(\frac{T}{L} \right)^2 \left(1 + 0.16 \left(\frac{C_B B}{T} \right) - 5.1 \left(\frac{B}{L} \right)^2 \right) \right)$ Clarke et al. (1982)
$Y_p = \frac{\partial Y}{\partial p}$	$Y_v (K_G - 0.5T)$ Assumption
$Y_r = \frac{\partial Y}{\partial r}$	$0.5\rho L^4 \left(-\pi \left(\frac{T}{L} \right)^2 \left(0.67 \left(\frac{B}{L} \right) - 0.0033 \left(\frac{B}{T} \right)^2 \right) \right)$ Clarke et al. (1982)
$Z_w = \frac{\partial Z}{\partial w}$	$-1.08m$ (Crude approximation from strip theory calculation) Journée (1992)
$Z_q = \frac{\partial Z}{\partial q}$	$-\frac{0.9I_{YY}}{L}$ (Crude approximation from strip theory calculation) Journée (1992)
$K_v = \frac{\partial K}{\partial v}$	Y_p
$K_p = \frac{\partial K}{\partial p}$	$-0.2I_{XX}$ (Crude approximation from strip theory calculation) Journée (1992)
$K_r = \frac{\partial K}{\partial r}$	$-0.0085I_{YY}$ (Crude approximation from strip theory calculation) Journée (1992)
$M_q = \frac{\partial M}{\partial q}$	$Z_q L$ Journée (1992)
$N_v = \frac{\partial N}{\partial v}$	Y_r Clarke et al. (1982)
$N_r = \frac{\partial N}{\partial r}$	$0.5\rho L^5 \left(-\pi \left(\frac{T}{L} \right)^2 \left(0.0833 + 0.017 \left(\frac{C_B B}{T} \right) - 0.0033 \left(\frac{B}{L} \right) \right) \right)$ Clarke et al. (1982)

Appendix B

Table 6
Approximation of added damping

X_{vv}	$\left[\frac{1.15C_B B}{L} - 0.18 \right] \frac{T}{L}$ Yoshimura and Masumoto (2011)
X_{vvv}	$\left[-\frac{6.68C_B B}{L} + 1.1 \right] \frac{T}{L}$ Yoshimura and Masumoto (2011)
X_{rr}	$\left[-\frac{0.085C_B B}{L} + 0.008 + \frac{x'_G Y_v}{T} \right] \frac{T}{L}$ Yoshimura and Masumoto (2011)
X'_{vr}	$[0.117Y_v'(0.5 + C_B)]$ Lee and Shin (1998)
Y'_v	$-\pi \left(\frac{T}{L} \right)^2 \left(1 + \frac{0.4C_B B}{T} \right)$ Clarke et al. (1982)
Y'_{vv}	$\left[-0.6469(1 - C_B) \left(\frac{T}{B} \right) + 0.0027 \right]$ Lee and Shin (1998)
Y'_r	$-\pi \left(\frac{T}{L} \right)^2 \left(-0.645 + 0.38 \frac{C_B B}{\pi T} \right)$ Norrbin (1970)
Y'_{rr}	$\left(-\frac{0.023C_B T}{B} + 0.0063 \right)$ Lee and Shin (1998)
Y'_{vrr}	$\left[\frac{1.5TC_B}{B} - 0.65 \right] \frac{T}{L}$ Kijima et al. (1990a)
Y'_{rrr}	$-\left(5.95(1 - C_B) \frac{T}{B} + 0.11 \right)$ Kijima et al. (1990a)
N'_v	$-\pi \left(\frac{T}{L} \right)^2 \left(0.5 + \frac{2.4T}{L} \right)$ Clarke et al. (1982)
N'_{vvv}	$\left(0.0348 - 0.5283(1 - C_B) \frac{T}{B} \right)$ Lee and Shin (1998)
N'_r	$-\pi \left(\frac{T}{L} \right)^2 \left(\frac{1.3192}{\pi} - \frac{0.68228 C_B}{\pi} - \frac{0.00019 L^2}{\pi T^2} \right)$ Khattab (1984)
N'_{rrr}	$\left[\frac{0.25C_B B}{L} - 0.056 \right] \frac{T}{L}$ Yoshimura and Masumoto (2011)

(continued on next page)

Table 6 (continued)

N'_{vvr}	$- \left(57.5 \left(\frac{C_B B}{L} \right)^2 - 18.4 \frac{C_B B}{L} + 1.6 \right)$ Kijima et al. (1990a)
N'_{vrt}	$0.5 \frac{C_B T}{B} - 0.05$ Kijima et al. (1990a)

Appendix C**Table 7**
Shallow water hydrodynamic derivatives formulation.

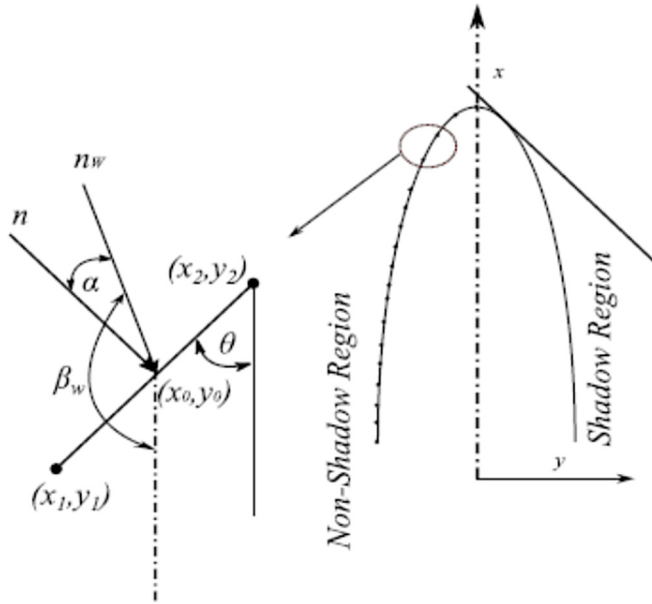
$Y_{vShallow}$	$gv^* Y_{Dep}$
$Y'_{vShallow}$	$gv^* Y'_{Dep}$
$N_{vShallow}$	$gv^* N_{Dep}$
$N'_{vShallow}$	$gnr^* N'_{Dep}$
$X'_{vvShallow}$	$fyv^* X'_{vvDep}$
$X'_{vvvvShallow}$	$fyv^* X'_{vvvvDep}$
$X'_{rrShallow}$	$fnr^* X'_{rrDep}$
$X'_{vtShallow}$	$fty^* X'_{vtDep}$
$Y'_{vvvShallow}$	$fyv^* Y'_{vvvDep}$
$N'_{vShallow}$	$f nv^* N'_{Dep}$
$N'_{vvvShallow}$	$fyv^* N'_{vvvDep}$
$Y'_{rrShallow}$	$f nr^* Y'_{rrDep}$
$Y'_{rrrShallow}$	$gnr^* Y'_{rrrDep}$
$N'_{rrrShallow}$	$gnr^* N'_{rrrDep}$
$Y'_{vrrShallow}$	$fyv^* Y'_{vrrDep}$
$Y'_{vrtShallow}$	$fyv^* Y'_{vrtDep}$
$gv = K_0 + \frac{2}{3}K_1 \frac{B_1}{T} + \frac{8}{15}K_2 \left(\frac{B_1}{T} \right)^2$	
$gnr = K_0 + \frac{8}{15}K_1 \frac{B_1}{T} + \frac{40}{105}K_2 \left(\frac{B_1}{T} \right)^2$	
$fyv = 1.5fnr - 0.5$	
$fyv = K_0 + \frac{2}{5}K_1 \frac{B_1}{T} + \frac{24}{105}K_2 \left(\frac{B_1}{T} \right)^2$	
$f nv = K_0 + K_1 \frac{B_1}{T} + K_2 \left(\frac{B_1}{T} \right)^2$	
$fnr = K_0 + \frac{1}{2}K_1 \frac{B_1}{T} + \frac{1}{3}K_2 \left(\frac{B_1}{T} \right)^2$, where $K_0 = 1 + \frac{0.0775}{H_T^2} - \frac{0.011}{H_T^3} + \frac{0.000068}{H_T^5}$	
$K_1 = -\frac{0.0643}{H_T} + \frac{0.0724}{H_T^2} - \frac{0.0113}{H_T^3} + \frac{0.0000767}{H_T^5}$	
$K_2 = \frac{0.0342}{H_T}$; if $\left\{ \frac{B}{T} > 4 : K_2 = \frac{0.137}{H_T} \frac{B}{T} H_T = \frac{H}{T} - 1 \right. B_1 = C_B B \left(1 + \frac{B}{L} \right)^2 ; B_2 = 0.83 \frac{B_1}{C_B}$	
$\left(-T_H + \frac{1}{0.4C_B B} \right) Y'_{Dep}$ (Kijima et al., 1990a) (Vantorre, 2001)	
$\left(-T_H + \frac{-0.26C_B B}{T} + 1.74 \right) Y'_{vvDep}$	
$Y'_{vvShallow}$	$\left(-T_H + \frac{-0.26C_B B}{T} + 1.74 \right) Y'_{vvDep}$
$Y'_{vShallow}$	$(1 + A_{1v} T_H + A_{2v} T_H^2 + A_{3v} T_H^3) Y'_{Dep}$
$N'_{vvShallow}$	$(1 + A_{1vv} T_H + A_{2vv} T_H^2 + A_{3vv} T_H^3) N'_{Dep}$
$N'_{vShallow}$	$\left(-T_H + \frac{1}{-14.28T} + 1.5 \right) N'_{Dep}$
$N'_{rrShallow}$	$(1 + A_{1rr} T_H + A_{2rr} T_H^2 + A_{3rr} T_H^3) N'_{Dep}$
$N'_{vvvShallow}$	$(1 + A_{1vvv} T_H + A_{2vvv} T_H^2 + A_{3vvv} T_H^3) N'_{Dep}$
$N'_{vrtShallow}$	$(1 + A_{1vrt} T_H + A_{2vrt} T_H^2 + A_{3vrt} T_H^3) N'_{Dep}$

(continued on next page)

Table 7 (continued)

$$\begin{aligned}
T_H = \frac{T}{H} A_{1_{Y_r}} &= -5.5 \left(\frac{C_B B}{T} \right)^2 + 26 \frac{C_B B}{T} - 31.5 A_{1_{N_{Y_r}}} = -15600(1 - C_B)^5 A_{1_{N_{Y_r}}} = 21500 \left((1 - C_B) \frac{T}{B} \right)^2 - 4800(1 - C_B) \frac{T}{B} + 220 A_{1_{N_{Y_r}}} = -240(1 - C_B) + 57 \\
A_{1_{N_{Y_r}}} &= -1960 \left((1 - C_B) \frac{T}{B} \right)^2 + 448(1 - C_B) \frac{T}{B} - 25 A_{1_{N_{Y_r}}} = 91 C_B \frac{T}{B} - 25 A_{1_{N_{Y_r}}} = 40 C_B \frac{B}{T} - 88 A_{2_{Y_r}} = 37 \left(\frac{C_B B}{T} \right)^2 - 185 \frac{C_B B}{T} + 230 A_{2_{Y_r}} = 116000(1 - C_B)^5 \\
A_{2_{Y_{N_r}}} &= -40800 \left((1 - C_B) \frac{T}{B} \right)^2 + 7500(1 - C_B) \frac{T}{B} - 274 A_{2_{N_{Y_r}}} = 1770(1 - C_B) - 413 A_{2_{N_{Y_r}}} = 12220 \left((1 - C_B) \frac{T}{B} \right)^2 - 2720(1 - C_B) \frac{T}{B} + 146 A_{2_{N_{Y_r}}} = -515 C_B \frac{B}{T} + 144 \\
A_{2_{N_{Y_r}}} &= -295 C_B \frac{B}{T} + 645 A_{3_{Y_r}} = -38 \left(\frac{C_B B}{T} \right)^2 + 197 C_B \frac{B}{T} - 250 A_{3_{Y_r}} = -128000(1 - C_B)^5 A_{3_{Y_{N_r}}} = -90800 \left((1 - C_B) \frac{T}{B} \right)^2 + 25500(1 - C_B) \frac{T}{B} - 1400 A_{3_{N_{Y_r}}} = -1980(1 - C_B) + 467 \\
A_{3_{N_{Y_r}}} &= -12160 \left((1 - C_B) \frac{T}{B} \right)^2 + 2650(1 - C_B) \frac{T}{B} - 137 A_{3_{N_{Y_r}}} = 508 C_B \frac{B}{T} - 143 A_{3_{N_{Y_r}}} = 312 C_B \frac{B}{T} - 678
\end{aligned}$$

Appendix D



The Figure illustrates the procedure of numerical integration along the non-shadow region of the waterline.

The two components of the normal vectors n are N_X and N_Y defined as

$$N_X = -(y_2 - y_1) N_Y = x_2 - x_1$$

The length of the element is,

$$dl = \sqrt{(N_X)^2 + (N_Y)^2}$$

The direction of the waves is defined with the vector n_w making an angle β_w as shown in the figure. Following waves are defined when β_w is zero. The components of the waves on a line each discretizes line-segments are:

$$N_{WX} = -\cos(180 - \beta_w) = \cos(\beta_w) N_{WY} = \sin(180 - \beta_w) = \sin(\beta_w)$$

The angle between the two vectors is α . Now the dot product of the normal vector and the wave vector will give:

$$\bar{n} \cdot \bar{n}_w = \frac{N_X N_{WX}}{dl} + \frac{N_Y N_{WY}}{dl}$$

If the dot product is positive then the line segment is considered to be in a non-shadow region, and therefore integration is performed along the line.

The angle α is obtained from the definition of the dot product as

$$\alpha = \cos^{-1}(\bar{n} \cdot \bar{n}_w)$$

References

- Acanfora, M., Matusiak, J., 2014. Quantitative assessment of ship behaviour in critical stern quartering seas. In: 14th International Ship Stability Workshop (ISSW). Kuala Lumpur, Malaysia, pp. 19–27.

Aksu, E., Köse, E., 2017. Evaluation of mathematical models for tankers' maneuvering motions. *J. ETA Marit. Sci.* 5, 95–109.

Amin, O.M., Hasegawa, K., 2010. Generalised mathematical model for ship manoeuvrability considering shallow water effect. In: Conference Proc, vol. 10. of Japan Society of Naval Architects and Ocean Engineers, pp. 531–534.

- Ankudinov, V.K., Miller, E.R., Jakobsen, B.K., Daggett, L.L., 1990. Manoeuvring performance of tug/barge assemblies in restricted waterways. Proceedings MARSIM & ICMS, pp. 515–525.
- Bailey, P., Hudson, D., Price, W., Temarel, P., 2002. Time simulation of manoeuvring and seakeeping assessments using a unified mathematical model. *Trans. R. Inst. Nav. Archit.* 144, 27–48.
- Beck, R.F., Cummins, W.E., Dalzell, J.F., Mandel, P., Webster, W.C., 1989. Principles of naval architecture. In: Lewis, E.V. (Ed.), Volume 3, SNAME. The Society of Naval Architects and Marine Engineers, p. 445.
- Bernitsas, M.M., Ray, D., Kinley, P., 1981. KT, KQ and Efficiency Curves for the Wageningen B-Series Propellers.
- Brix, J.E., 1993. Manoeuvring Technical Manual. Seehafen-Verl., Hamburg.
- Chilcote, G., el Moctar, O., 2018. A numerical method for manoeuvring simulation in regular waves. *Ocean Eng.* 434–444.
- Chroni, D., Liu, S., Plessas, T., Papanikolaou, A., 2015. Simulation of the maneuvering behavior of ships under the influence of environmental forces. Towards Green Marine Technology and Transport, pp. 111–119.
- Clarke, D., Gedling, P., Hine, G., 1982. The application of manoeuvring criteria in hull design using linear theory. *R. Inst. Nav. Archit.* 45–68.
- Eloot, K., Vantorre, M., Delefortrie, G., Quadflieg, F., 2015. Validation of ship manoeuvring in shallow water through free-running tests. In: ASME 34th International Conference on Ocean, Offshore and Arctic Engineering. American Society of Mechanical Engineers Digital Collection.
- Emsa, 2019. Annual Overview of Marine Casualties and Incidents 2019. European Maritime Safety Agency, Lisbon, Portugal.
- Faltinsen, O.M., 1990. Sea Loads on Ships and Offshore Structures. Cambridge University press.
- Faltinsen, O., Zhao, R., 1991. Numerical predictions of ship motions at high forward speed. *Philos. Trans. R. Soc. London. Ser. A Phys. Eng. Sci.* 334, 241–252. <https://doi.org/10.1098/rsta.1991.0011>.
- Fossen, T.I., 2002. Marine Control Systems. Book.
- Fossen, T.I., 2011. Handbook of Marine Craft Hydrodynamics and Motion Control, Handbook of Marine Craft Hydrodynamics and Motion Control.
- Frank, W., 1967. Oscillation of cylinders in or bellow the free surface of deep fluids. David W. Taylor Nav. Sh. Res. Dev. Center.
- Gavrilin, S., Steen, S., 2018. Global sensitivity analysis and repeated identification of a modular maneuvering model of a passenger ferry. *Appl. Ocean Res.* 74, 1–10.
- Hirano, M., Takashina, J., 1980. A calculation of ship turning motion taking coupling effect due to heel into consideration, 59. Transaction of The West-Japan Society of Naval Architect, pp. 71–81.
- Hirdaris, S.E., Lee, Y., Mortola, G., Incevik, A., Turan, O., Hong, S.Y., Kim, B.W., Kim, K.H., Bennett, S., Miao, S.H., Temarel, P., 2016. The influence of nonlinearities on the symmetric hydrodynamic response of a 10,000 TEU Container ship. *Ocean Eng.* 111, 166–178.
- Holtrop, J., Mennen, G.G.J., 1982. An approximate power prediction method. *Int. Shipbuild. Prog.* 29, 166–170.
- IMO, 2013. Annex 16, Resolution MEPC. 232(65)-2013 Interim guidelines for determining minimum propulsion power to maintain the manoeuvrability of ships in adverse conditions, Annex 16. Resolution MEPC 232 (65).
- Inoue, S., Hirano, M., Kijima, K., 1981. Hydrodynamic derivatives on ship manoeuvring. *Int. Shipbuild. Prog.* 28, 112–125.
- ITTC, 2017a. Report of the manoeuvring committee. Proceedings of the 28th International Towing Tank Conference. Wuxi, China.
- ITTC, 2017b. Preparation, conduct and analysis of speed/power trials. Appendix K, 'Raven Shallow Water Correction,' in: ITTC Recommended Proced. Guidel. (2017), pp. 71–73, 7.5-04-01-01.1, Revision 5.
- Journée, J., 1992. Quick strip theory calculations in ship design. PRADS'92 Conf. Pract. Des. Ships.
- Khattab, O., 1984. Multiple Regression Analysis of the Hydrodynamic Derivatives for Manoeuvring Equations, BSRA Report No. W1090.
- Kijima, K., Katsuno, T., Nakiri, Y., Furukawa, Y., 1990a. On the manoeuvring performance of a ship with the parameter of loading condition. *J. Soc. Nav. Archit. Jpn.* 168, 141–148.
- Kijima, K., Nakiri, Y., Tsutsui, Y., Matsunaga, M., 1990b. Prediction method of ship manoeuvrability in deep and shallow waters. International Conference on Marine Simulation and Ship Maneuverability. MARSIM '90, p. 311.
- Kim, Y.G., Kim, S.Y., Kim, H.T., Lee, S.W., Yu, B.S., 2007. Prediction of the manoeuvrability of a large container ship with twin propellers and twin rudders. *J. Mar. Sci. Technol.* 12, 130–138.
- Kim, S., Korgesaar, M., Ahmadi, N., Taimuri, G., Kujala, P., Hirdaris, S., 2020. A fluid structure interaction model for the idealization of dynamic response of ships subject to collision and grounding. *Mar. Struct.* (under rev).
- Kujala, P., Hänninen, M., Arola, T., Ylitalo, J., 2009. Analysis of the marine traffic safety in the Gulf of Finland. *Reliab. Eng. Syst. Saf.* 94, 1349–1357.
- Lee, H.-Y., Shin, S.-S., 1998. The Prediction of ship's manoeuvring performance in initial design stage. *Dev. Mar. Technol.* 11, 633–639.
- Lewandowski, E.M., 2004. The dynamics of marine craft maneuvering and seakeeping. Advanced Series on Ocean Engineering ume 22.
- Liu, J., Hekkenberg, R., 2017. Sixty years of research on ship rudders: effects of design choices on rudder performance. *Ships Offshore Struct.* 12, 495–512.
- Liu, J., Hekkenberg, R., Rotteveel, E., Hopman, H., 2015. Literature review on evaluation and prediction methods of inland vessel manoeuvrability. *Ocean Eng.* 106, 458–471.
- Liu, S., Shang, B., Papanikolaou, A., Bolbot, V., 2016. Improved formula for estimating added resistance of ships in engineering applications. *J. Mar. Sci. Appl.* 15, 442–451.
- Luhmann, H., 2009. Integrated Flooding and Standard for Stability and Crises Management. FLOODSTAND deliverable No. D1.1b.
- Matusiak, J., 2000. Ship Buoyancy and Stability. In: Finnish), fourth ed. Otatioto, Otatioto, Espoo.
- Matusiak, J.E., 2017. Dynamics of a Rigid Ship. Aalto University. <https://aaltodoc.aalto.fi/bitstream/handle/123456789/24408/isbn9789526072623.pdf>.
- Matusiak, J.E., Stigler, C., 2012. Ship roll motion in irregular waves during a turning circle maneuver. 11th International Conference on Stability of Ships and Ocean Vehicles, pp. 291–298.
- Molland, A., Turnock, S., 2007. Marine rudders and control surfaces. *Marine Rudders and Control Surfaces*.
- Mucha, P., 2017. On Simulation-Based Ship Maneuvering Prediction in Deep and Shallow Water. Univ. Duisburg-Essen.
- Norrbin, N.H., 1970. Theory and observation on the use of a mathematical model for ship maneuvering in deep and confined waters. In: Proceedings of the 8th Symposium on Naval Hydrodynamics, Pasadenca, 1970.
- Pagiaziti, A., Mallaga, E., Eliopoulou, E., Zaraphonitis, G., Hamann, R., 2015. Statistics of collision, grounding and contact accidents of passenger and container ships. *Proc. 5th Symp. Sh. Oper. Manag. Econ.* 8–29.
- Papanikolaou, A., Fournarakis, N., Chroni, D., Liu, S., Plessas, T., 2016. Simulation of the maneuvering behavior of ships in adverse weather conditions. 31st Symposium on Naval Hydrodynamics, pp. 11–16.
- Perez, T., Mak, T., Armstrong, T., Ross, A., Fossen, T.I., 2007. Validation of a 4DOF manoeuvring model of a high-speed vehicle-passenger trimaran. FAST 23–27, 9th International Conference on Fast Sea Transportation. 2007.
- Raven, H.C., 2016. A new correction procedure for shallow-water effects in ship speed trials. PRADS 2016 - Proceedings of the 13th International Symposium on PRActical Design of Ships and Other Floating Structures.
- Rotteveel, E., 2013. Investigation of Inland Ship Resistance, Propulsion and Manoeuvring Using Literature Study and Potential Flow Calculations. Tech. Univ. Delft.
- Sakamoto, T., Baba, E., 1986. Minimization of resistance of slowly moving full hull forms in short waves. Proceedings of Sixteenth Symposium on Naval Hydrodynamics, pp. 598–613.
- Sakamoto, N., Carrica, P.M., Stern, F., 2012. URANS simulations of static and dynamic maneuvering for surface combatant: Part 1. Verification and validation for forces, moment, and hydrodynamic derivatives. *J. Mar. Sci. Technol.* <https://doi.org/10.1007/s00773-012-0178-x>.
- Schröder-Hinrichs, J.U., Hollnagel, E., Baldauf, M., 2012. From Titanic to Costa Concordia—a century of lessons not learned. *WMU J. Marit. Aff.* 11, 151–167.
- Seo, M.G., Kim, Y., 2011. Numerical analysis on ship maneuvering coupled with ship motion in waves. *Ocean Eng.* 38, 1934–1945.
- SIMMAN, 2020. n.d. SIMMAN 2020 (workshop on verification and validation of ship manoeuvring simulation methods) [WWW Document]. URL http://simman2019.kr/contents/Ship_data_summary.php .
- Söding, H., 1982. Prediction of ship steering capabilities. *Schiffstechnik* 29, 3–29.
- Sprenger, F., Maron, A., CEHIPAR, Delefortrie, G., Flanders, H.R., Cura-Hochbaum, A., Technische, U.B., Fathi, D., Marintek, 2015. Mid-term Review of Tank Test Results, D3.2 of EU FP7 project on Energy Efficient Safe SHip OPERAtion (SHOPERA).
- Sprenger, F., Maron, A., Delefortrie, G., Zwijnsvoorde, T. Van, Cura-Hochbaum, A., Lengwinat, A., Papanikolaou, A., 2017. Experimental studies on seakeeping and maneuverability of ships in adverse weather conditions. *J. Sh. Res.* 61, 131–152.
- Spyrou, K.J., Thompson, J.M.T., Spyrou, K.J., Thompson, J.M.T., 2000. The nonlinear dynamics of ship motions: a field overview and some recent developments. *Philos. Trans. R. Soc. London. Ser. A Math. Phys. Eng. Sci.* 358, 1733–1734.
- Stählerberg, K., Goerlandt, F., Ehlers, S., Kujala, P., 2013. Impact scenario models for probabilistic risk-based design for ship-ship collision. *Mar. Struct.* 33, 238–264.
- Stern, F., Agdrup, K., Kim, S.Y., Hochbaum, A.C., Rhee, K.P., Quadflieg, F., Perdon, P., Hino, T., Broglia, R., Gorski, J., 2011. Experience from SIMMAN 2008-The first workshop on verification and validation of ship maneuvering simulation methods. *J. Sh. Res.* 55, 135–147.
- Sukas, O.F., Kinaci, O.K., Bal, S., 2019a. Theoretical background and application of MANSIM for ship maneuvering simulations. *Ocean Eng.* 192, 106239.
- Sukas, O.F., Kinaci, O.K., Bal, S., 2019b. System-based prediction of maneuvering performance of twin-propeller and twin-rudder ship using a modular mathematical model. *Appl. Ocean Res.* 84, 145–162. <https://doi.org/10.1016/j.apor.2019.01.008>.
- Taimuri, G., Mikkola, T., Matusiak, J., Kujala, P., Hirdaris, S., 2019. The influence of hydrodynamic assumptions on ship maneuvering. In: 22nd Numerical Towing Tank Symposium (NuTTS 2019)-Tomar, Portugal, p. 6.
- Thorby, D., 2008. Structural Dynamics and Vibration in Practice, Structural Dynamics and Vibration in Practice.
- Tillig, F., Ringsberg, J.W., 2018. A 4 DOF simulation model developed for fuel consumption prediction of ships at sea. *Ships Offshore Struct.* 14, 112–120.
- Vantorre, M., 2001. Manoeuvring coefficients for a container carrier in shallow water: an evaluation of semi-empirical formulae. In: Mini Symposium on Prediction of Ship Manoeuvring Performance, vol. 18. October 2001, Tokyo, Japan.
- Vantorre, M., Eloot, K., Delefortrie, G., Lataire, E., Candries, M., Verwilligen, J., 2017. Maneuvering in shallow and confined water. Encyclopedia of Maritime and Offshore Engineering, pp. 1–17.
- Varsta, P.M., Kajaste-Rudnitski, J., Matusiak, J.E., 2004a. Dynamics of ship grounding. The Ninth International Symposium of Practical Design on Ships and Other Floating Structures, (PRADS). Technical University of Hamburg-Harburg, Lubeck-Travemunde, Germany, pp. 465–473.
- Varsta, P.M., Kajaste-Rudnitski, J., Matusiak, J.E., 2004b. Mechanics of ship grounding. The 14th International Offshore and Polar Engineering Conference (ISOPE). Toulon, France, pp. 569–577.

- Yasukawa, H., Hirata, N., 2013. Maneuverability and hydrodynamic derivatives of ships traveling in heeled condition. *J. Japan Soc. Nav. Archit. Ocean Eng.* <https://doi.org/10.2534/jjasnaoe.17.19>.
- Yasukawa, H., Yoshimura, Y., 2015. Introduction of MMG standard method for ship maneuvering predictions. *J. Mar. Sci. Technol.* 20, 37–52.
- Yoon, H., 2009. Phase-averaged Stereo-PIV Flow Field and Force/moment/motion Measurements for Surface Combatant in PMM Maneuvers. University of Iowa.
- Yoshimura, Y., Masumoto, Y., 2011. Hydrodynamic force database with medium high speed merchant ships including fishing vessels and investigation into a manoeuvring prediction method. *J. Japan Soc. Nav. Archit. Ocean Eng.* 14, 63–73.
- Yu, Z., Amdahl, J., 2016. Full six degrees of freedom coupled dynamic simulation of ship collision and grounding accidents. *Mar. Struct.* 47, 1–22.
- Yu, D., Wang, L., Yeung, R.W., 2019. Experimental and numerical study of ship-to-ship interactions in overtaking manoeuvres. *Proc. R. Soc. A Math. Phys. Eng. Sci.* 475, 20180748.